<u>Electronic Supplementary Information</u>

Observation of "de Vries-like" properties in bent-core molecules

Supreet Kaur,†[a] Abinash Barthakur,†[b] Golam Mohiuddin,†[a]§ Santosh Prasad Gupta,[c] Surajit Dhara,[b] Santanu Kumar Pal[*a]

[a]Department of Chemical Sciences, Indian Institute of Science Education and Research (IISER) Mohali, Sector-81, Knowledge City, Manauli 140306, India

[b]School of Physics, University of Hyderabad, Hyderabad-500046, India

[c]Department of Physics, Patna University, Patna-800005, India

§Present address: Department of Chemistry, University of Science & Technology Meghalaya, Ri-Bhoi, Meghalaya-793101, India

†Joint first authors

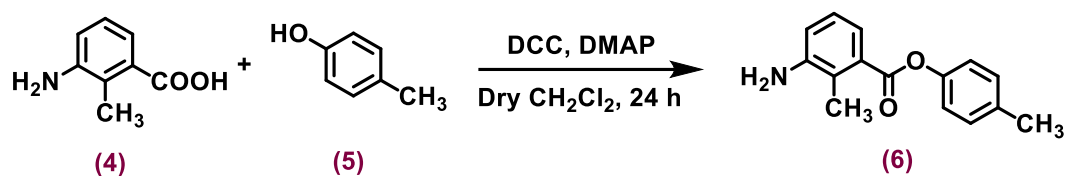Email: skpal@iisermohali.ac.in

Table of contents

1. **Synthesis and characterization:**

- **General procedure for synthesis of compounds 3.n**:

*The procedure has been reported elsewhere[1,2] and reproduced below for the convenience of readers:*

"An ethanolic solution of 4-hydroxybenzoic acid (1 equiv.) was refluxed with potassium hydroxide (KOH) (2.5 equiv.) solution with further addition of alkyl bromide ($C_nH_{2n+1}Br$) (1.2 equiv.). After 6 h of stirring, 10% KOH was added (for base hydrolysis) and refluxed for

another 3 h. The reaction mixture was then poured in acid water for neutralization. The white solid appeared on constant stirring and was filtered and collected as the product (4-n-alkoxybenzoic acid (**1.n**); yield: 82-85 %). The 4-n-alkoxybenzoic acid was further dissolved in dry dichloromethane (CH_2Cl_2) in an inert nitrogen atmosphere followed by addition of N, N'-dicyclohexylcarbodiimide (DCC) (1.2 equiv.) and catalytic amount of 4-dimethylaminopyridine (DMAP). After 0.5 h, 4-hydroxybenzaldehyde (**2**) (1 equiv.) was added. The reaction mixture was stirred for 24 h at room temperature. The precipitate of dicyclohexylurea (DCU) was removed by filtration and the solvent CH_2Cl_2 was evaporated to get the crude product. The reaction mixture was purified by column chromatography using silica (100-200 mesh) eluting with a mixture of hexane-ethyl acetate. The product **3.n** was obtained as a white solid. Yield: 63-65 %

All the homologues of **3.n** with varying the number of carbon atoms in the alkoxy chain (n = 10, 12, 14, 16, 18) were synthesized adopting the same procedure as above with appropriate amount of alkyl bromides."

^{1}H NMR of **3.18** (400 MHz, CDCl$_3$, δ in ppm): δ = 10.02 (s, 1H, -CHO), 8.14 (d, 2H, J = 8.0 Hz, Ar-H), 7.97 (d, 2H, J = 8.0 Hz, Ar-H), 7.40 (d, 2H, J = 8.0 Hz, Ar-H), 6.98 (d, 2H, J = 8.0 Hz, Ar-H), 4.05 (t, 2H, J = 6.0 Hz, -OCH$_2$-), 1.86-1.79 (m, 2H, -CH$_2$-), 1.51-1.44 (m, 2H, -CH$_2$-), 1.38-1.26 (m, 28H, -(CH$_2$)$_{14}$-), 0.88 (t, 3H, J = 6.0 Hz, -CH$_3$). ^{13}C NMR of **3.18** (100 MHz, CDCl$_3$, δ in ppm): δ = 14.17, 22.72, 25.76, 25.99, 29.09, 29.39, 29.46, 29.58, 29.62, 29.64, 29.69, 29.73, 31.95, 68.41, 114.43, 120.77, 122.64, 131.27, 132.45, 133.88, 155.91, 163.88, 164.27, 191.06.

- **General procedure for synthesis of compound p-tolyl 3-amino-2-methylbenzoate**:

The procedure has been reported elsewhere[1,2] and reproduced below for the convenience of readers:

"3-Amino-2-methylbenzoic acid (**4**) (1 equiv.) was dissolved in dry dichloromethane (CH_2Cl_2) in an inert nitrogen atmosphere followed by addition of N, N'-dicyclohexylcarbodiimide (DCC) (1.2 equiv.) and catalytic amount of 4-dimethylaminopyridine (DMAP). p-cresol (**5**) (1 equiv.) was added after 0.5 h of stirring. The reaction mixture was stirred for 24 h at room temperature. The precipitate of dicyclohexylurea (DCU) was removed by filtration and the solvent CH_2Cl_2 was evaporated to get the solid crude product. The solid was recrystallized 2-3 times using absolute ethanol to give a brown semi-solid product p-tolyl 3-amino-2-methylbenzoate (**6**). Yield: 85 %" ^{1}H NMR (400 MHz, CDCl$_3$, δ in ppm): δ = 7.52 (d, 1H, J = 8.0 Hz, Ar-H), 7.27-7.24 (m, 2H, Ar-H), 7.18-7.11 (m, 3H, Ar-H), 6.91 (d, 1H, J = 8.0 Hz, Ar-H), 3.81 (s, 2H, -NH$_2$), 2.46 (s, 3H, -CH$_3$), 2.40 (s, 3H, -CH$_3$).

- **General procedure for synthesis of compounds 1/n:**

The procedure has been reported elsewhere[1,2] and reproduced below for the convenience of readers:

"The final compounds were prepared by refluxing a mixture of ethanolic solution of **3.n** (1 equiv.) with **6** (1 equiv.) and a few drops of glacial acetic acid as catalyst for 4 h. The precipitated product was Schiff base. It was dissolved in hot boiling ethanol and the insoluble white solid was collected as the pure product (**1/n**). Yield: 75-78 %"
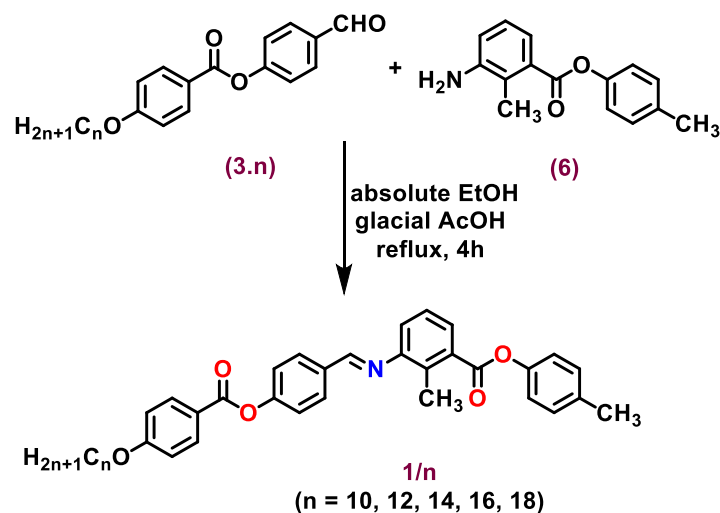
Five compounds (**1/10**, **1/12**, **1/14**, **1/16**, **1/18**) have been synthesized by varying the terminal alkoxy chain.

Structural characterization

p-tolyl (E)-3-((4-((4-(decyloxy)benzoyl)oxy)benzylidene)amino)-2-methylbenzoate (Compound 1/10):

^{1}H NMR (400 MHz, CD$_2$Cl$_2$, δ in ppm): δ = 8.40 (s, 1H, -CH=N-), 8.15 (dd, 2H, J = 8.0, 4.0 Hz, Ar-H), 8.03 (dd, 2H, J = 6.8, 1.8 Hz, Ar-H), 7.92 (d, 1H, J = 8.0 Hz, Ar-H), 7.38-7.34 (m, 3H, Ar-H), 7.27-7.24 (m, 2H, Ar-H), 7.17 (d, 1H, J = 6.9 Hz, Ar-H), 7.11 (dd, 2H, J = 6.4, 2.0 Hz, Ar-H), 7.01 (dd, 2H, J = 6.9, 2.0 Hz, Ar-H), 4.06 (t, 2H, J = 6.0 Hz, -OCH$_2$-), 2.63 (s, 3H, -CH$_3$), 2.39 (s, 3H, -CH$_3$), 1.86-1.79 (m, 2H, -CH$_2$-), 1.52-1.44 (m, 2H, -CH$_2$-), 1.39-1.29 (m, 12H, -(CH$_2$)$_6$-), 0.89 (t, 3H, J = 8.0 Hz, -CH$_3$).

^{13}C NMR (100 MHz, CDCl$_3$, δ in ppm): δ = 14.14, 15.34, 20.93, 22.70, 25.99, 29.09, 29.33, 29.37, 29.56, 31.90, 68.38, 114.37, 121.45, 122.02, 122.38, 126.33, 127.91, 130.01, 130.11, 130.32, 132.39, 133.71, 134.25, 135.51, 148.67, 152.40, 153.66, 159.30, 163.73, 164.64, 166.48.

FT-IR (cm^{-1}): C=C aromatic stretching at 1607 cm^{-1}, HC=N stretching of imine at 1631 cm^{-1}, C=O stretching band of ester at 1729 cm^{-1}, C-H stretching of alkanes at 2923 cm^{-1}.

UV-vis (nm): 275 nm, 329 nm.
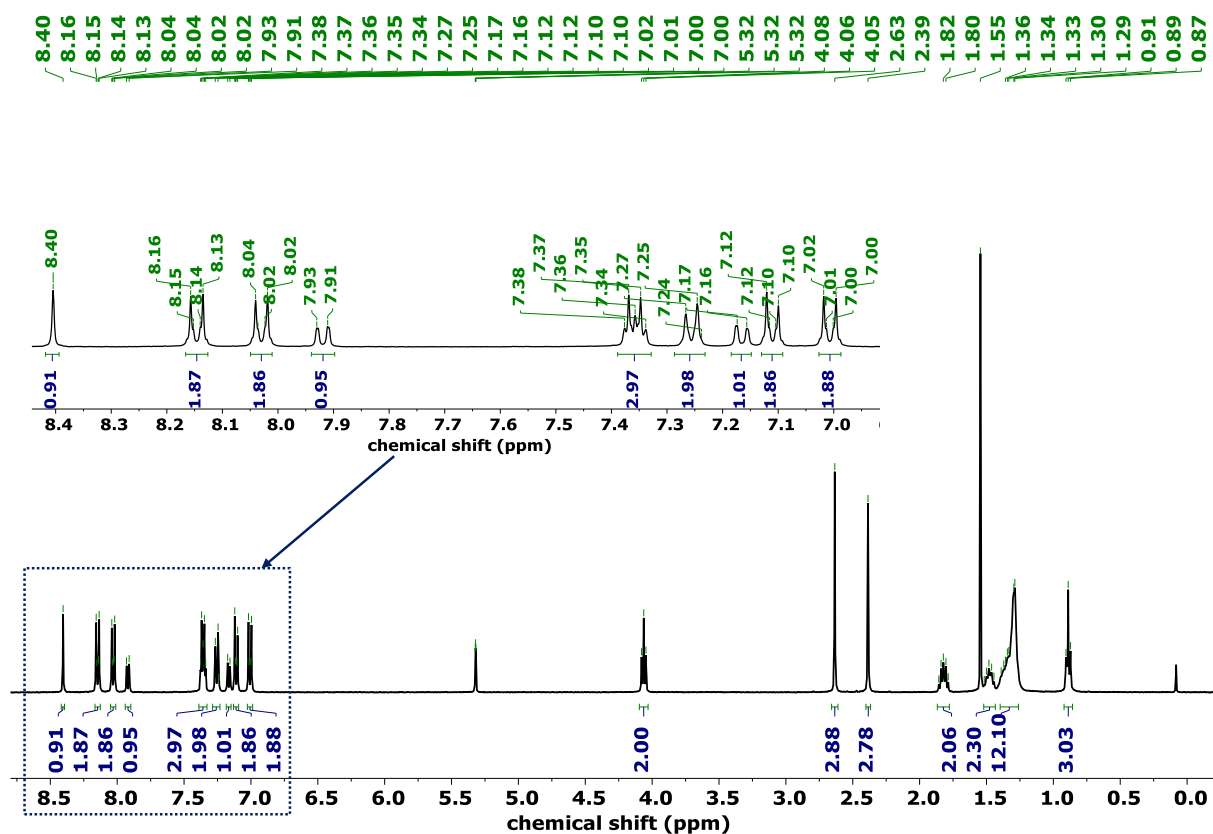
Fig. S1 ^{1}H NMR of compound **1/10**.

Fig. S2 ^{13}C NMR of compound **1/10**.

M+H (theoretical) = 606.3219
M+H (observed) = 606.3223
Error = 0.7 ppm
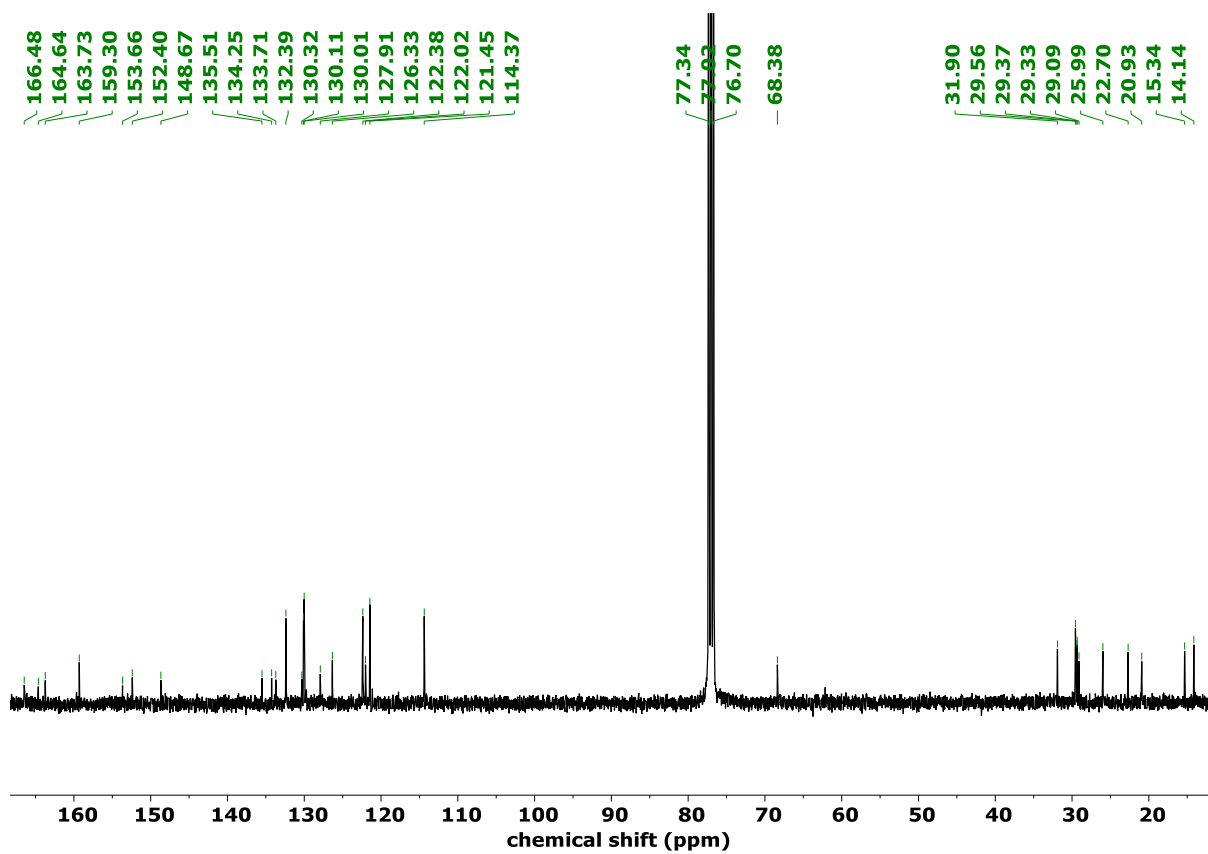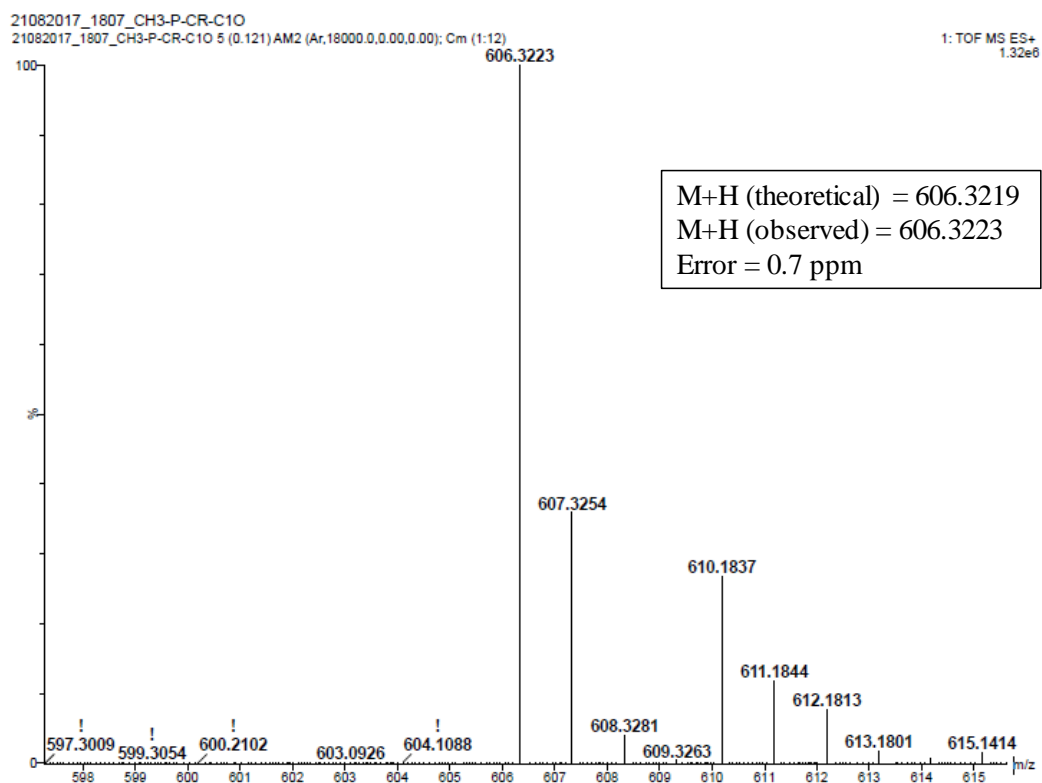
Fig. S3 ESI spectrum of compound **1/10**.

p-tolyl (E)-3-((4-((4-(dodecyloxy)benzoyl)oxy)benzylidene)amino)-2-methylbenzoate (Compound 1/12):

^{1}H NMR (400 MHz, CDCl$_3$, δ in ppm): δ = 8.37 (s, 1H, -CH=N-), 8.16 (d, 2H, J = 8.0 Hz, Ar-H), 8.01 (d, 2H, J = 8.0 Hz, Ar-H), 7.95 (d, 1H, J = 8.0 Hz, Ar-H), 7.36-7.32 (m, 3H, Ar-H), 7.24 (d, 2H, J = 8.0 Hz, Ar-H), 7.14-7.11 (m, 3H, Ar-H), 6.99 (d, 2H, J = 8.0 Hz, Ar-H), 4.05 (t, 2H, J = 6.0 Hz, -OCH$_2$-), 2.66 (s, 3H, -CH$_3$), 2.38 (s, 3H, -CH$_3$), 1.86-1.80 (m, 2H, -CH$_2$-), 1.51-1.44 (m, 2H, -CH$_2$-), 1.39-1.27 (m, 16H, -(CH$_2$)$_8$-), 0.89 (t, 3H, J = 6.0 Hz, -CH$_3$).

^{13}C NMR (100 MHz, CDCl$_3$, δ in ppm): δ = 14.14, 15.34, 20.92, 22.70, 25.98, 29.09, 29.36, 29.56, 29.59, 29.64, 29.66, 31.92, 68.37, 114.37, 121.12, 121.45, 122.02, 122.37, 126.34, 130.01, 130.11, 130.32, 132.39, 133.71, 134.25, 135.51, 148.67, 152.40, 153.66, 159.30, 163.73, 164.64, 166.48.

FT-IR (cm^{-1}): C=C aromatic stretching at 1609 cm^{-1}, HC=N stretching of imine at 1631 cm^{-1}, C=O stretching band of ester at 1728 cm^{-1}, C-H stretching of alkanes at 2924 cm^{-1}.

UV-vis (nm): 275 nm, 329 nm.
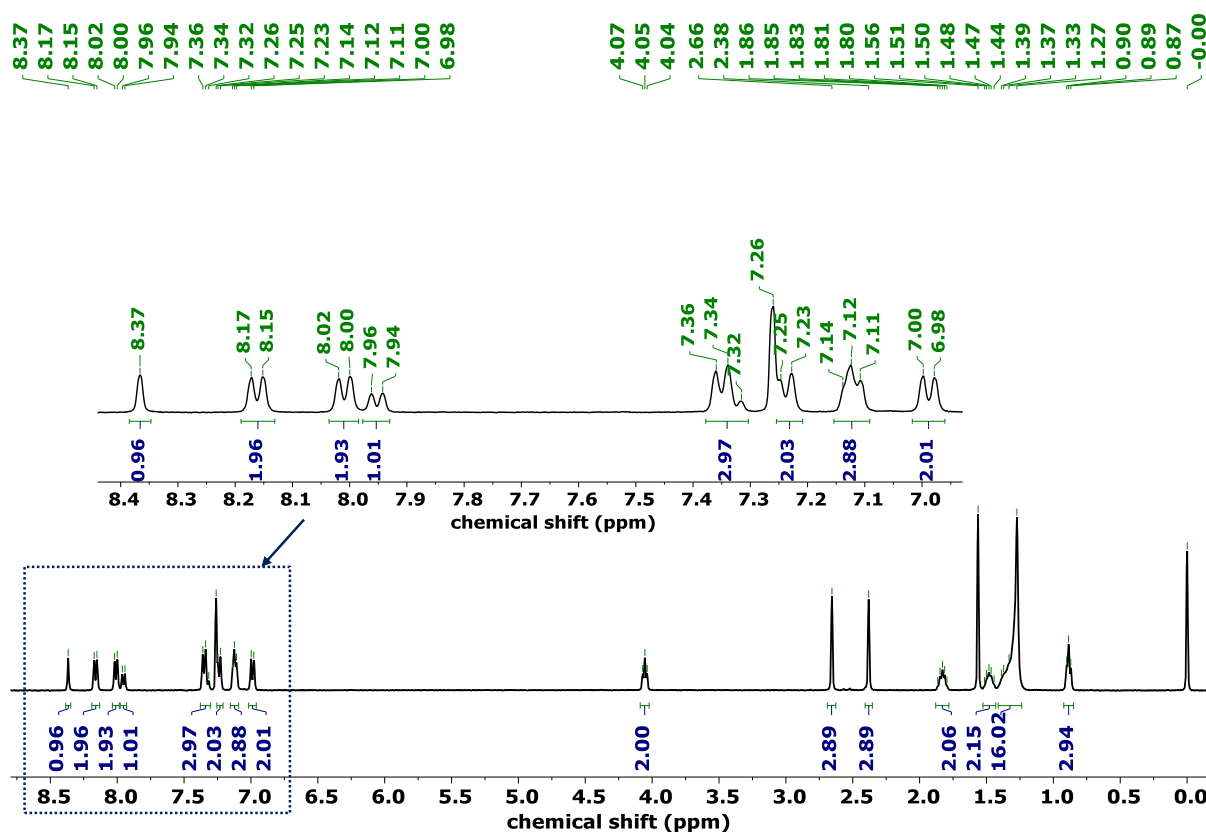
Fig. S4 ^{1}H NMR of compound **1/12**.

Fig. S5 ^{13}C NMR of compound **1/12**.

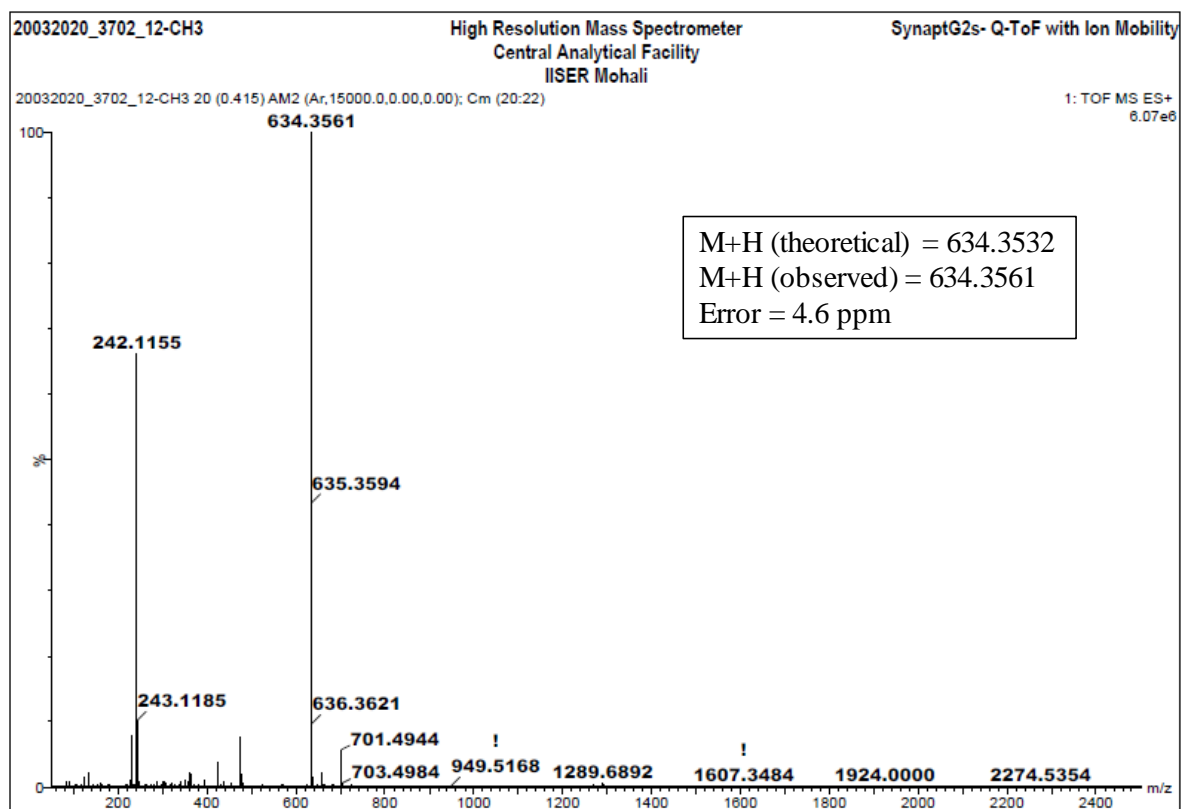M+H (theoretical) = 634.3532
M+H (observed) = 634.3561
Error = 4.6 ppm
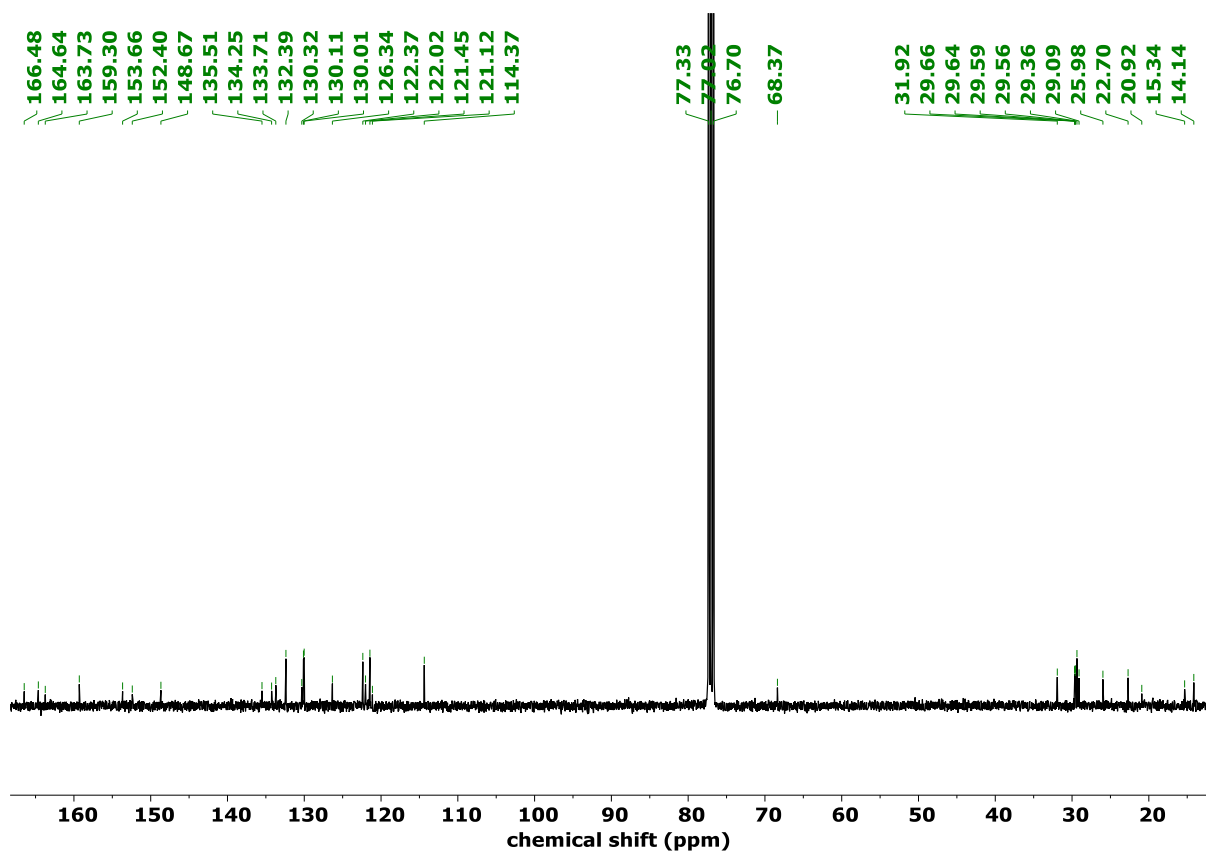
Fig. S6 ESI spectrum of compound **1/12**.

p-tolyl (E)-2-methyl-3-((4-((4-(tetradecyloxy)benzoyl)oxy)benzylidene)amino)benzoate (Compound 1/14):

^{1}H NMR (400 MHz, CDCl$_3$, δ in ppm): δ = 8.37 (s, 1H, -CH=N-), 8.16 (d, 2H, J = 8.0 Hz, Ar-H), 8.01 (d, 2H, J = 8.0 Hz, Ar-H), 7.95 (d, 1H, J = 8.0 Hz, Ar-H), 7.36-7.32 (m, 3H, Ar-H), 7.24 (d, 2H, J = 8.0 Hz, Ar-H), 7.13-7.11 (m, 3H, Ar-H), 6.99 (d, 2H, J = 8.0 Hz, Ar-H), 4.05 (t, 2H, J = 6.0 Hz, -OCH$_2$-), 2.66 (s, 3H, -CH$_3$), 2.38 (s, 3H, -CH$_3$), 1.87-1.79 (m, 2H, -CH$_2$-), 1.52-1.44 (m, 2H, -CH$_2$-), 1.41-1.27 (m, 20H, -(CH$_2$)$_{10}$-), 0.88 (t, 3H, J = 6.0 Hz, -CH$_3$).

^{13}C NMR (100 MHz, CDCl$_3$, δ in ppm): δ = 14.14, 15.34, 20.92, 22.70, 25.98, 29.09, 29.37, 29.56, 29.60, 29.67, 29.68, 29.70, 31.93, 68.37, 114.36, 121.12, 121.44, 122.01, 122.37, 126.33, 127.91, 130.01, 130.04, 130.10, 130.32, 132.38, 133.70, 134.25, 135.50, 148.67, 152.39, 153.66, 159.29, 163.73, 164.63, 166.46.

FT-IR (cm^{-1}): C=C aromatic stretching at 1608 cm^{-1}, HC=N stretching of imine at 1633 cm^{-1}, C=O stretching band of ester at 1730 cm^{-1}, C-H stretching of alkanes at 2923 cm^{-1}.

UV-vis (nm): 275 nm, 329 nm.

Fig. S7 ^{1}H NMR of compound **1/14**.

166.46
164.63
163.73
159.29
153.66
152.39
148.67
135.50
134.25
133.70
132.38
130.32
130.10
130.04
130.01
127.91
126.33
122.37
122.01
121.44
121.12
114.36

77.33
77.03
76.70

68.37

31.93
29.70
29.68
29.67
29.60
29.56
29.37
29.09
25.98
22.70
20.92
15.34
14.14

chemical shift (ppm)

Fig. S8 ^{13}C NMR of compound **1/14**.

04062018_2246_CH3-P-CR-14
04062018_2246_CH3-P-CR-14 12 (0.260) AM2 (Ar,18000.0,0.00,0.00); ABS; Cm (2:38-53:97)

1: TOF MS ES+
1.00e8

662.3818

M+H (theoretical) = 662.3845
M+H (observed) = 662.3818
Error = 4.0 ppm

663.3855

664.3888

665.3943

123.0882
225.1914
242.1136
315.2388
448.2924
536.1609   610.1793
781.1816   855.2007
902.5057 1003.2349

m/z

Fig. S9 ESI spectrum of compound **1/14**.

p-tolyl (E)-3-((4-((4-(hexadecyloxy)benzoyl)oxy)benzylidene)amino)-2-methylbenzoate (Compound 1/16):

^{1}H NMR (400 MHz, CDCl$_3$, δ in ppm): δ = 8.37 (s, 1H, -CH=N-), 8.16 (d, 2H, J = 8.0 Hz, Ar-H), 8.01 (d, 2H, J = 8.0 Hz, Ar-H), 7.95 (d, 1H, J = 8.0 Hz, Ar-H), 7.36-7.32 (m, 3H, Ar-H), 7.24 (d, 2H, J = 8.0 Hz, Ar-H), 7.14-7.11 (m, 3H, Ar-H), 6.99 (d, 2H, J = 8.0 Hz, Ar-H), 4.05 (t, 2H, J = 6.0 Hz, -OCH$_2$-), 2.66 (s, 3H, -CH$_3$), 2.38 (s, 3H, -CH$_3$), 1.86-1.79 (m, 2H, -CH$_2$-), 1.52-1.44 (m, 2H, -CH$_2$-), 1.38-1.26 (m, 24H, -(CH$_2$)$_{12}$-), 0.88 (t, 3H, J = 8.0 Hz, -CH$_3$).

^{13}C NMR (100 MHz, CDCl$_3$, δ in ppm): δ = 14.13, 15.33, 20.92, 22.70, 25.99, 29.10, 29.37, 29.57, 29.60, 29.67, 29.70, 31.93, 68.38, 114.38, 121.15, 121.45, 122.00, 122.37, 126.33, 127.90, 130.01, 130.10, 130.35, 132.39, 133.72, 134.25, 135.49, 148.70, 152.40, 153.68, 159.28, 163.74, 164.62, 166.46.

FT-IR (cm^{-1}): C=C aromatic stretching at 1608 cm^{-1}, HC=N stretching of imine at 1630 cm^{-1}, C=O stretching band of ester at 1727 cm^{-1}, C-H stretching of alkanes at 2922 cm^{-1}.

UV-vis (nm): 275 nm, 329 nm.
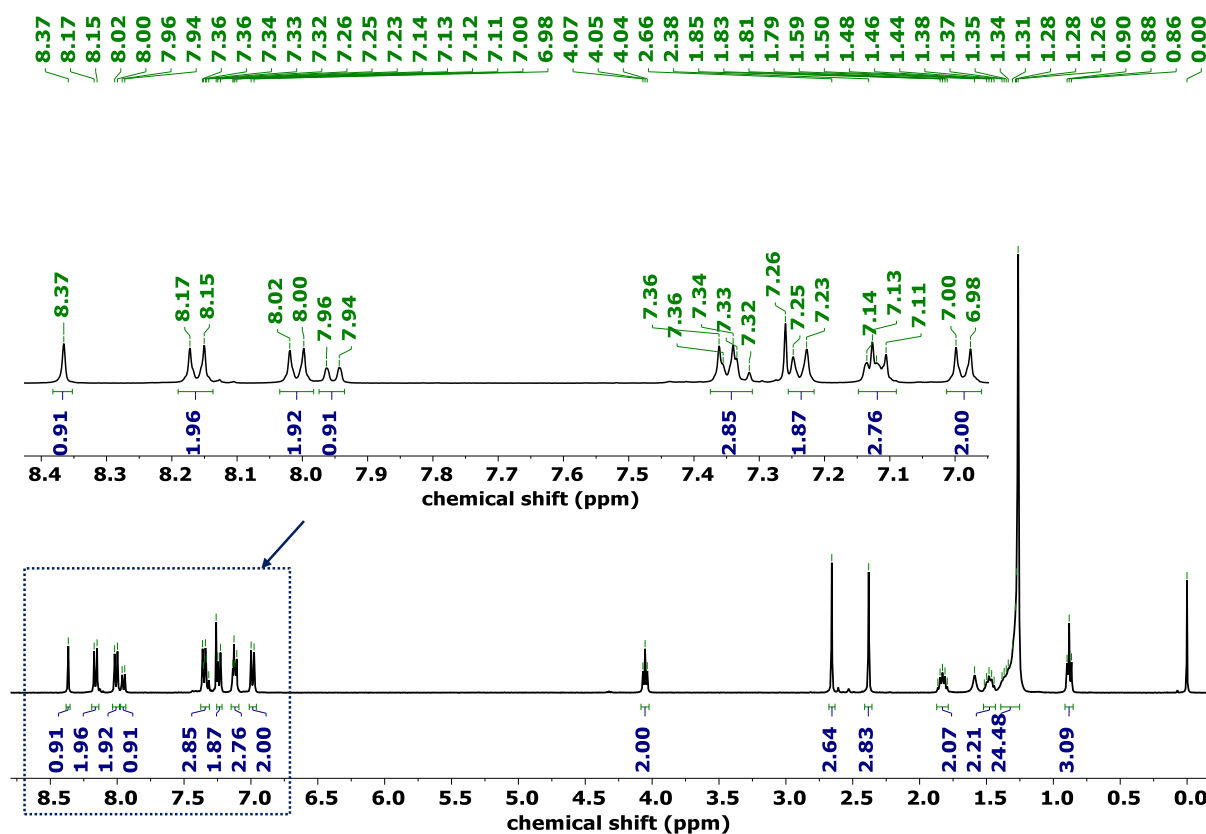
Fig. S10 ^{1}H NMR of compound **1/16**.
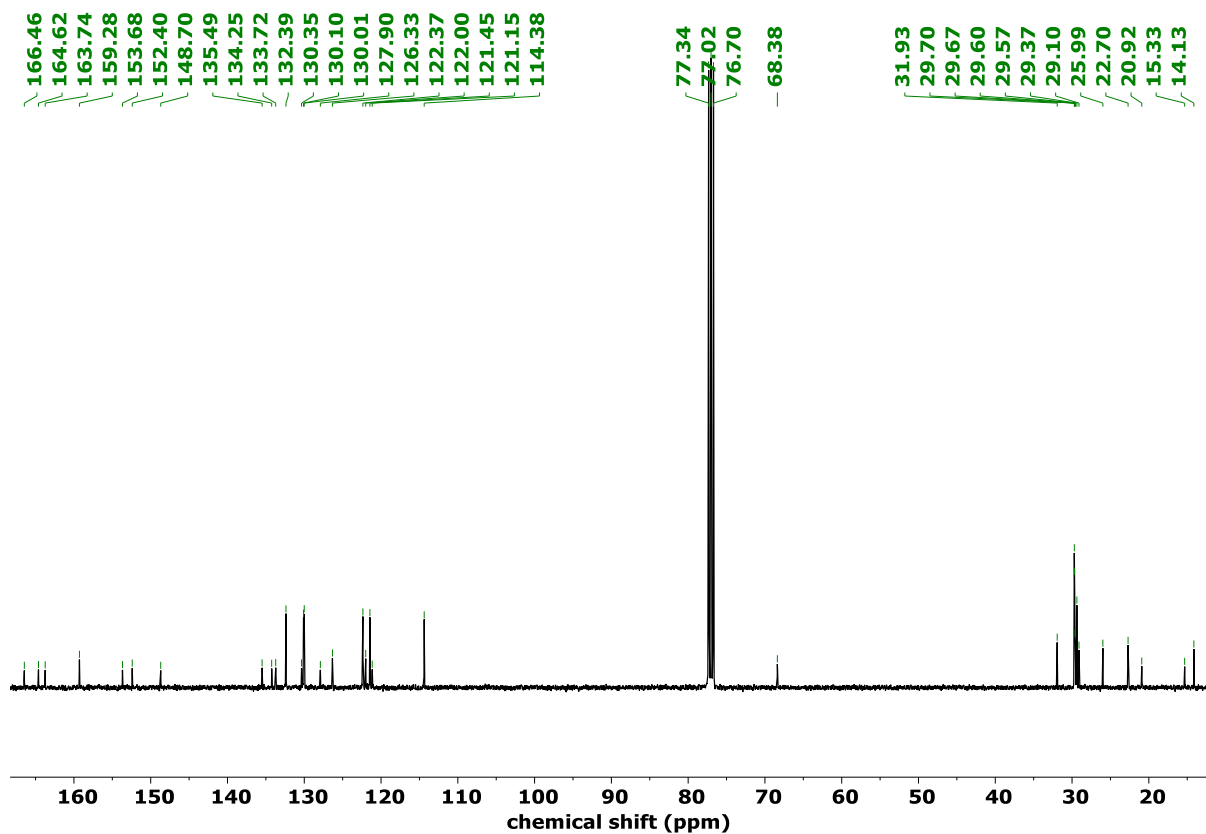
Fig. S11 ^{13}C NMR of compound **1/16**.

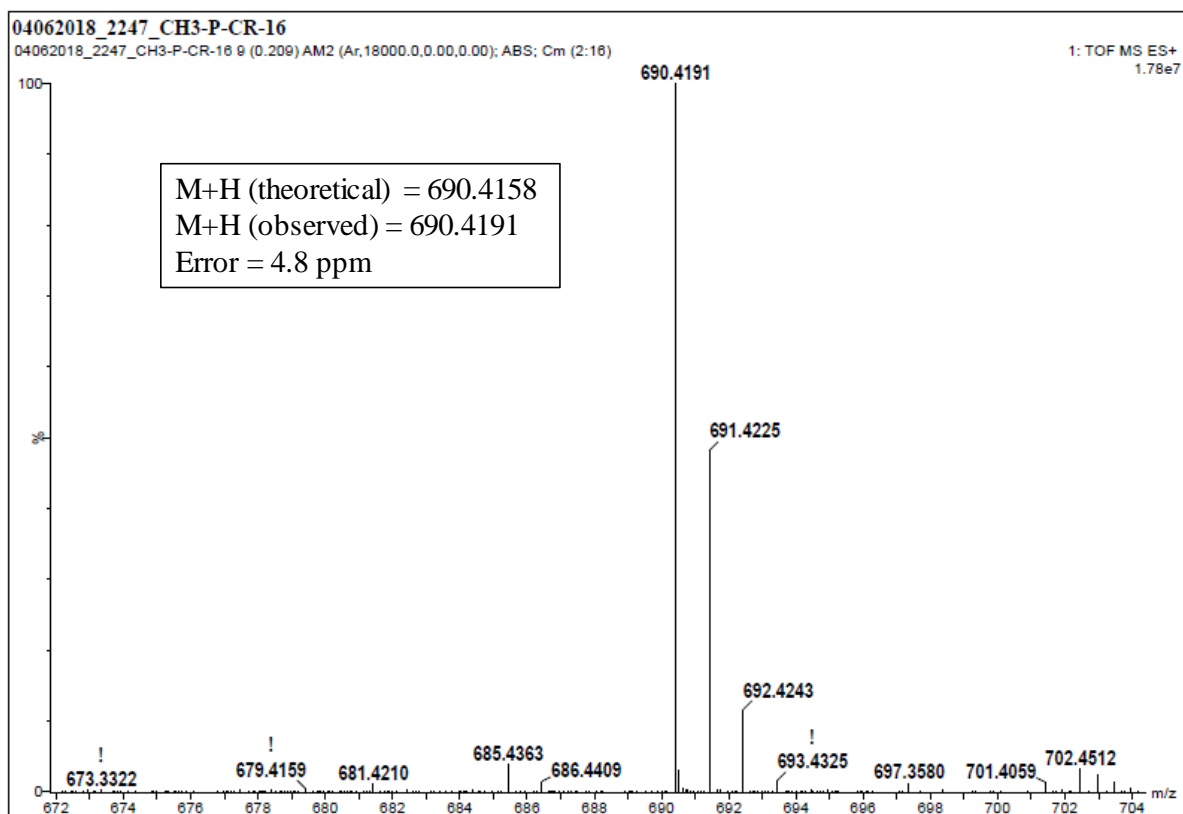M+H (theoretical) = 690.4158
M+H (observed) = 690.4191
Error = 4.8 ppm

Fig. S12 ESI spectrum of compound **1/16**.

p-tolyl (E)-2-methyl-3-((4-((4-(octadecyloxy)benzoyl)oxy)benzylidene)amino)benzoate (Compound 1/18):

^{1}H NMR (400 MHz, CDCl$_3$, δ in ppm): δ = 8.37 (s, 1H, -CH=N-), 8.16 (d, 2H, J = 8.0 Hz, Ar-H), 8.01 (d, 2H, J = 8.0 Hz, Ar-H), 7.95 (d, 1H, J = 8.0 Hz, Ar-H), 7.36-7.31 (m, 3H, Ar-H), 7.24 (d, 2H, J = 8.0 Hz, Ar-H), 7.14-7.11 (m, 3H, Ar-H), 6.99 (d, 2H, J = 8.0 Hz, Ar-H), 4.05 (t, 2H, J = 6.0 Hz, -OCH$_2$-), 2.66 (s, 3H, -CH$_3$), 2.38 (s, 3H, -CH$_3$), 1.86-1.79 (m, 2H, -CH$_2$-), 1.52-1.44 (m, 2H, -CH$_2$-), 1.39-1.26 (m, 28H, -(CH$_2$)$_{14}$-), 0.88 (t, 3H, J = 8.0 Hz, -CH$_3$).

^{13}C NMR (100 MHz, CDCl$_3$, δ in ppm): δ = 14.14, 15.34, 20.92, 22.70, 25.98, 29.09, 29.37, 29.57, 29.60, 29.67, 29.71, 31.93, 68.37, 114.37, 114.43, 121.13, 121.45, 122.01, 122.37, 122.62, 126.33, 127.91, 130.01, 130.10, 130.32, 131.25, 132.39, 133.71, 134.26, 135.50, 148.67, 152.40, 153.66, 159.29, 163.73, 164.63, 166.47.

FT-IR (cm^{-1}): C=C aromatic stretching at 1605 cm^{-1}, HC=N stretching of imine at 1629 cm^{-1}, C=O stretching band of ester at 1728 cm^{-1}, C-H stretching of alkanes at 2922 cm^{-1}.

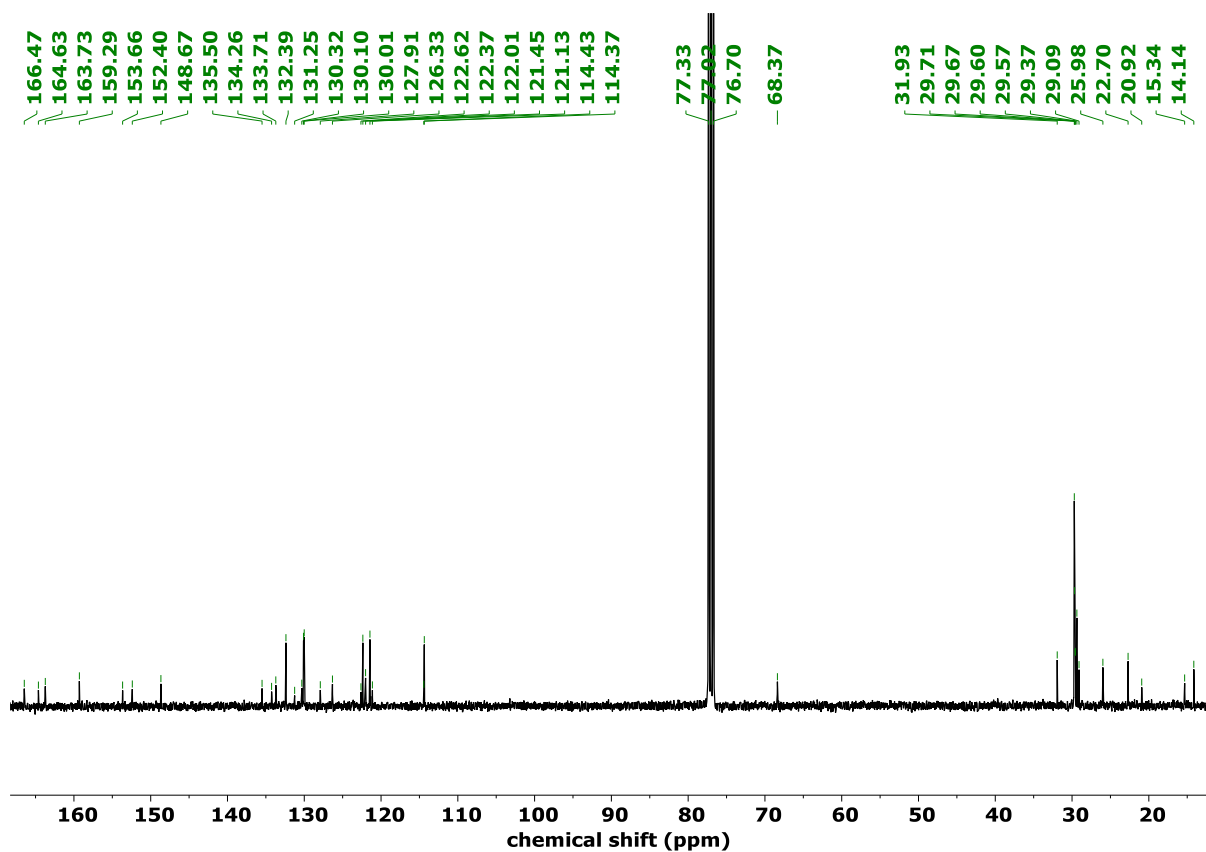**UV-vis (nm):** 275 nm, 329 nm.
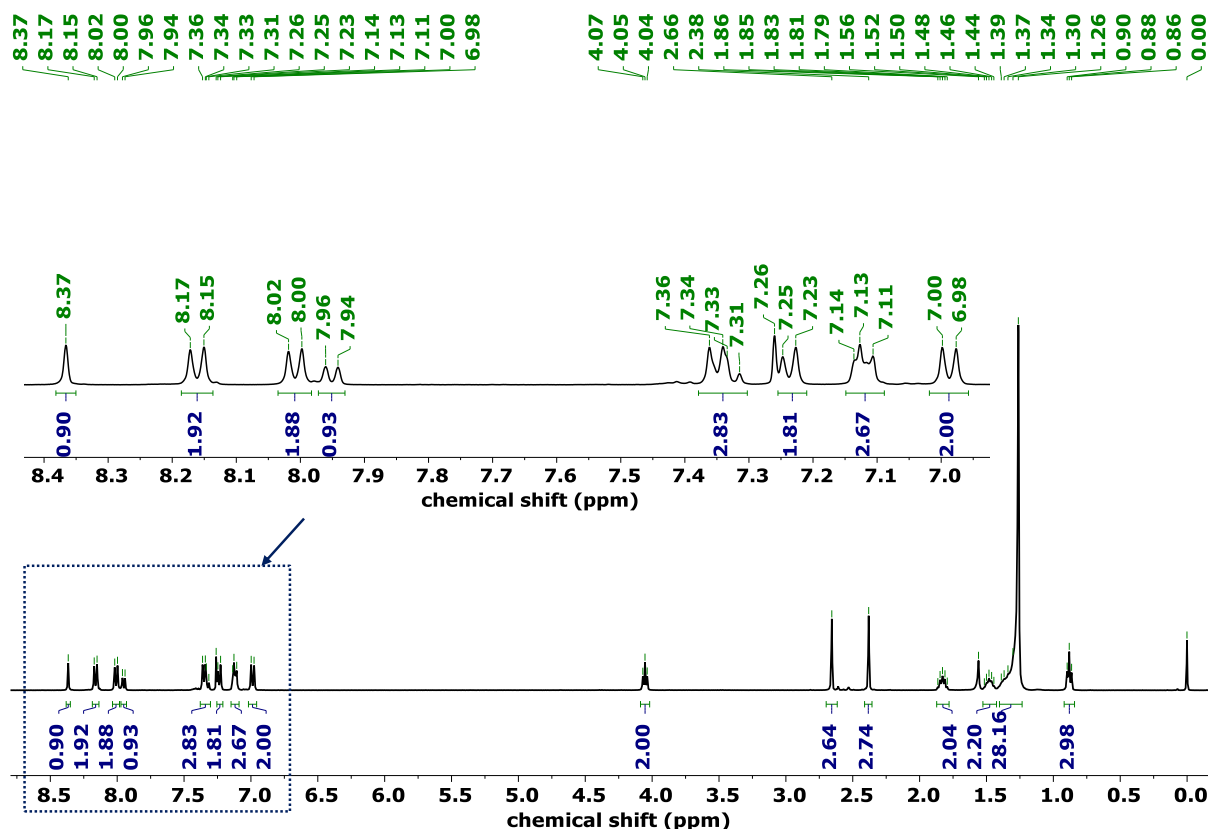
Fig. S13 ^{1}H NMR of compound **1/18**.

Fig. S14 ^{13}C NMR of compound **1/18**.

M+H (theoretical) = 718.4471
M+H (observed) = 718.4446
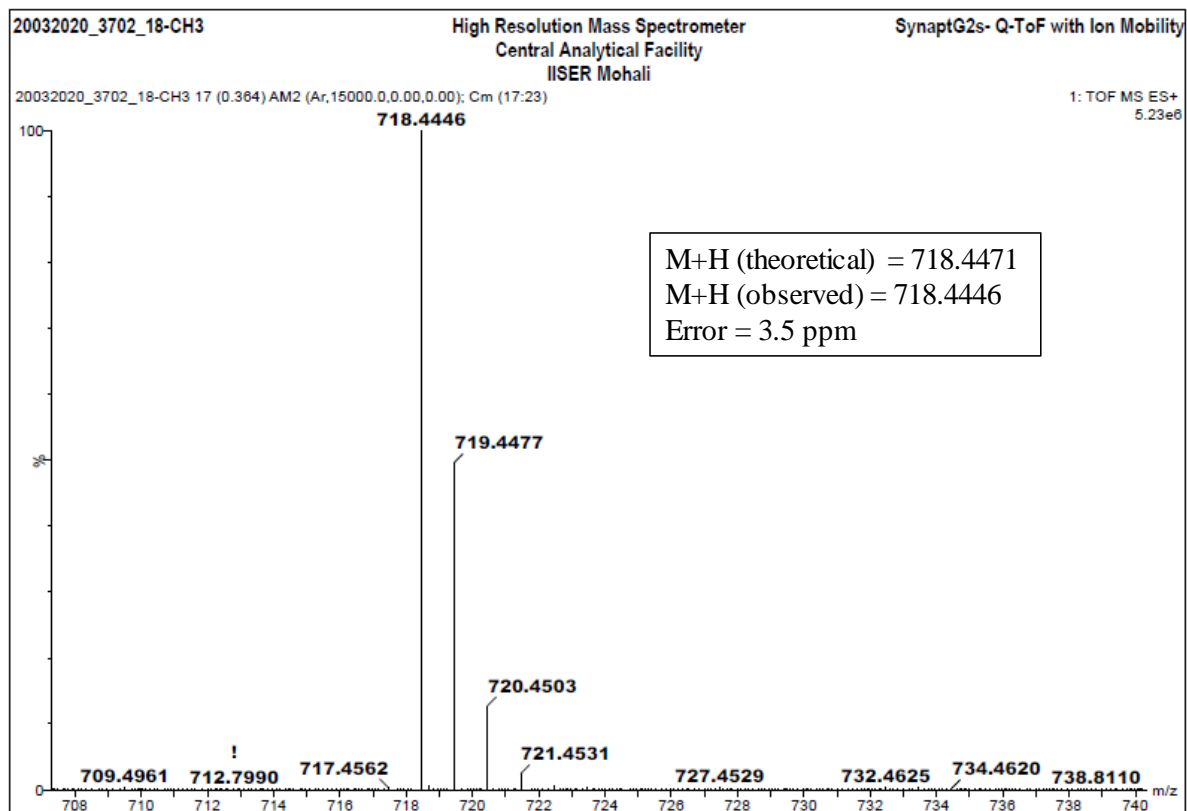Error = 3.5 ppm

Fig. S15 ESI spectrum of compound **1/18**.

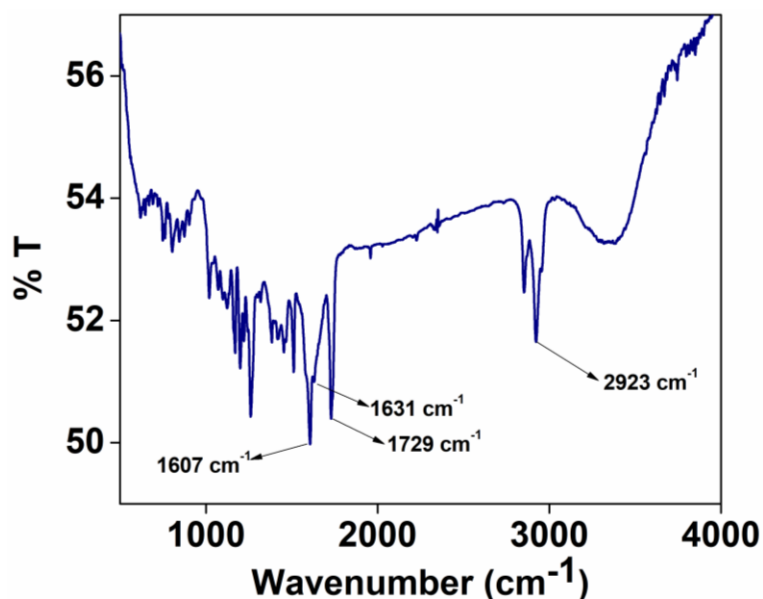## 2. Fourier-transform infrared (FT-IR) spectroscopy:

Fig. S16 FT-IR spectrum of a representative compound **1/10**.

3. Ultraviolet-visible (UV-vis) spectroscopy:

The UV absorption spectroscopic studies were carried out on a representative compound **1/10** in dichloromethane (CH_2Cl_2) solution of 10^{-4} M concentration to obtain the information regarding absorption maxima. The compound exhibited maximum absorption peak at 275 nm (4.5 eV, $\varepsilon \sim 9500$ L mol^{-1} cm^{-1}) and a minimum at 329 nm.

The absorption band with large molar absorption coefficient (λ_{max} = 275 nm) corresponds to the π-π* transition contributed from the **3.n** intermediate series. The band at 329 nm reflects the π-π* transition of the highly π-conjugated system with substituted phenyl benzoate unit as the core contributed from the intermediate **6** (Fig. S17). Similar results were found for the other homologues of **1/n** series (where n = 12, 14, 16, 18) as well.
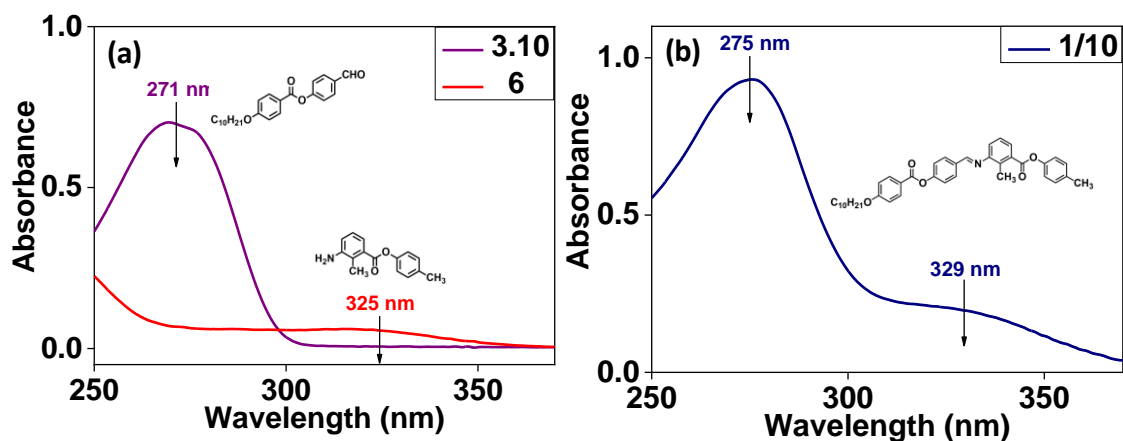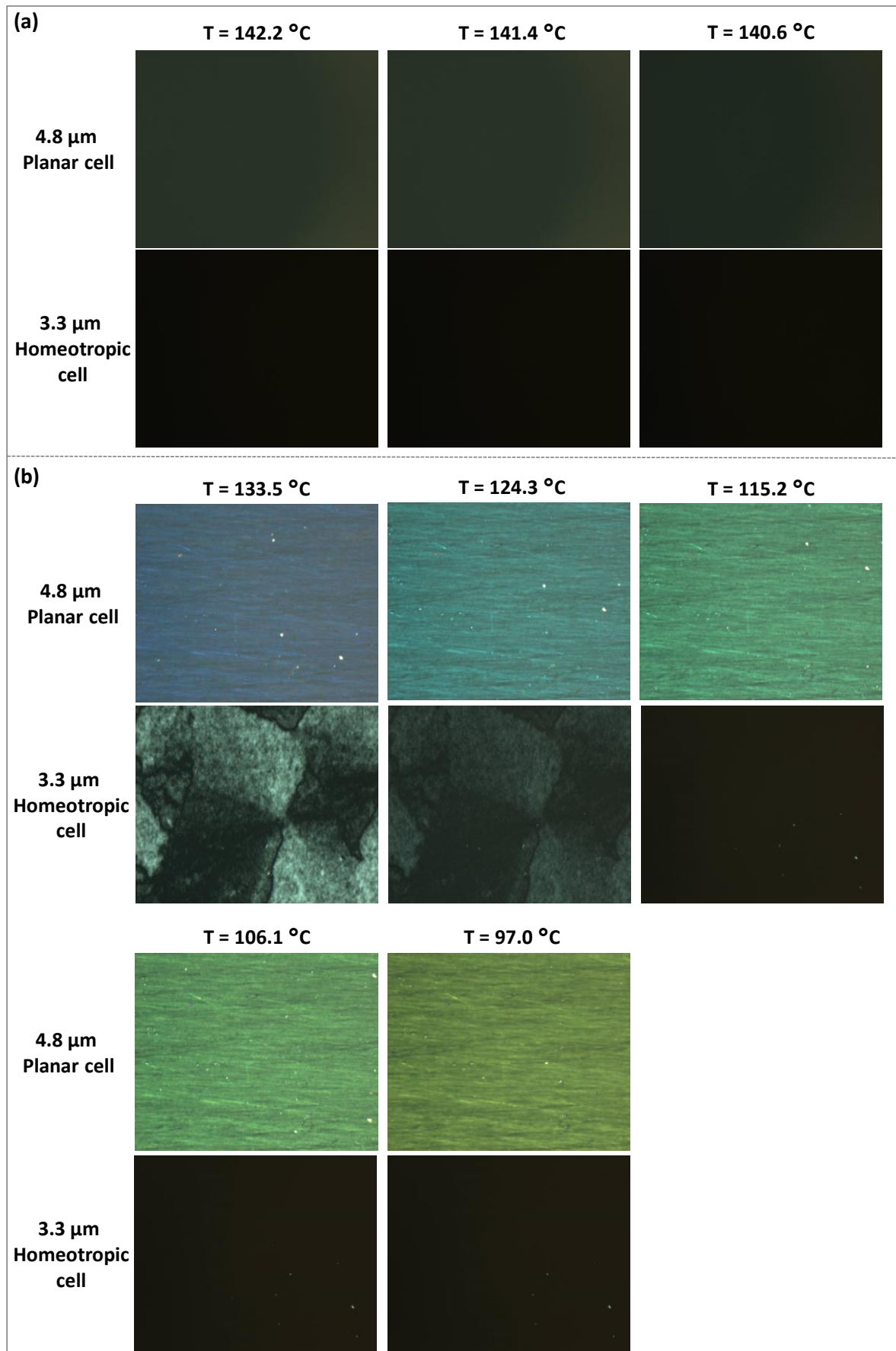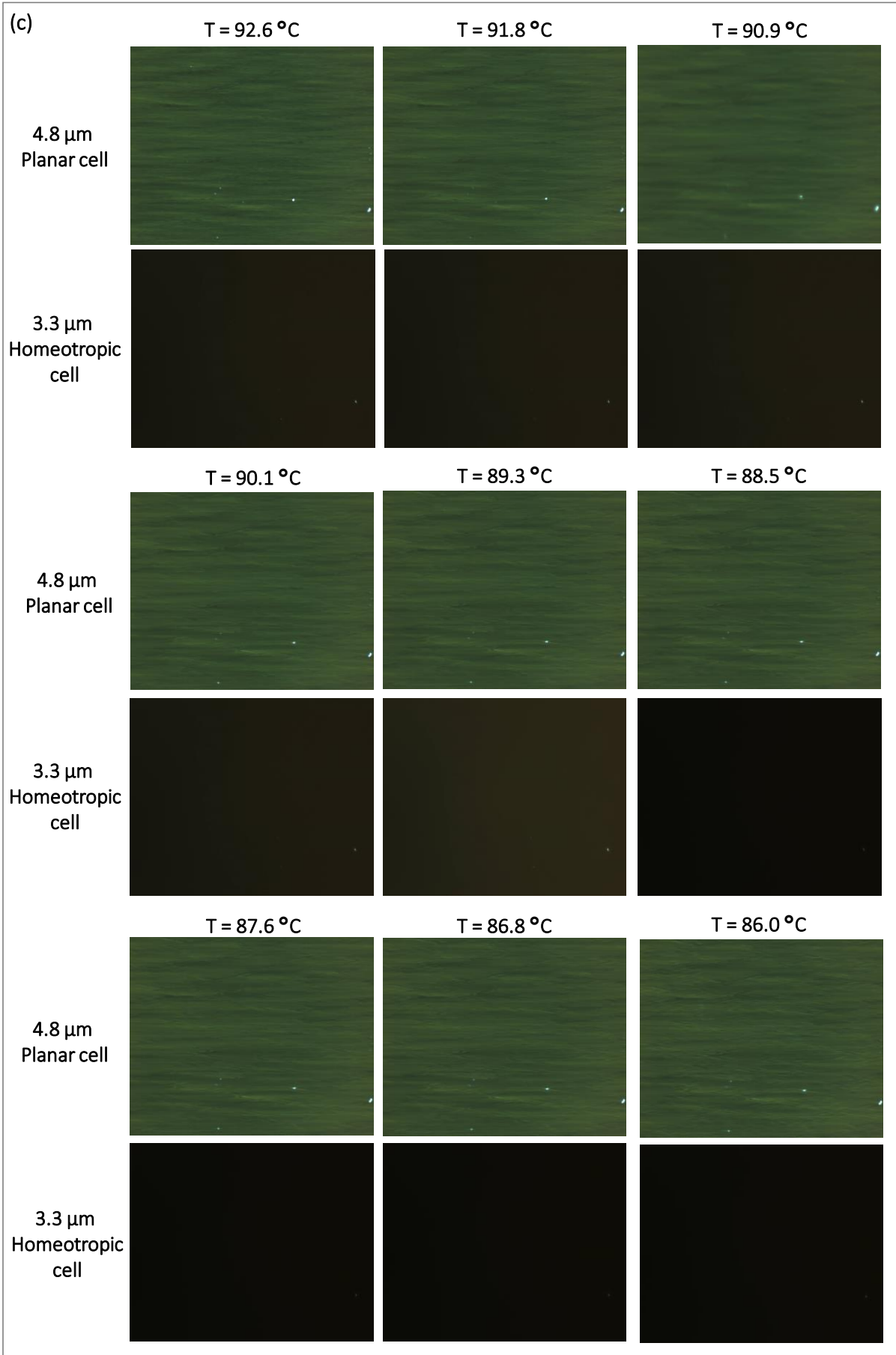

Fig. S17 Representative UV-visible plots of the (a) intermediates (**3.10** and **6**) and (b) final compound (**1/10**).

4. Polarizing Optical Microscopy (POM) studies:

For suitable designation of the mesophases, all the compounds were studied under a polarizing optical microscope (with crossed polarizers) under different anchoring conditions such as homogeneous (planar) and homeotropic anchoring cells with different cell gaps purchased from INSTEC, USA. The transition from SmA to SmC was proved with the help of textural changes as well as the change in the layer spacing (discussed in XRD studies section).
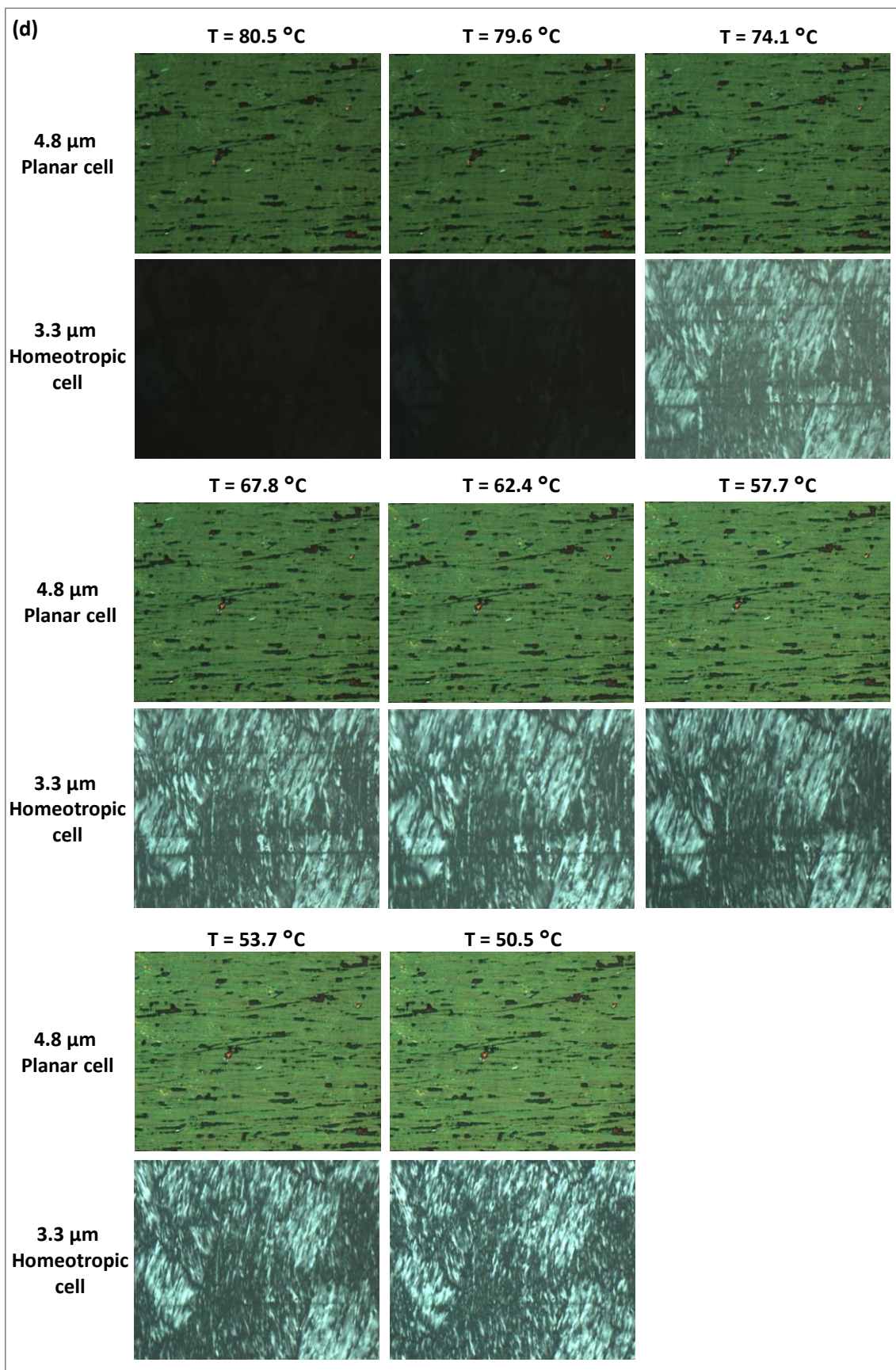
Compound **1/10**:

(a)

	T = 142.2 °C	T = 141.4 °C	T = 140.6 °C
4.8 µm Planar cell			
3.3 µm Homeotropic cell			

(b)

	T = 133.5 °C	T = 124.3 °C	T = 115.2 °C
4.8 µm Planar cell			
3.3 µm Homeotropic cell			

	T = 106.1 °C	T = 97.0 °C
4.8 µm Planar cell		
3.3 µm Homeotropic cell		

(c)

	T = 92.6 °C	T = 91.8 °C	T = 90.9 °C
4.8 μm Planar cell			
3.3 μm Homeotropic cell			

	T = 90.1 °C	T = 89.3 °C	T = 88.5 °C
4.8 μm Planar cell			
3.3 μm Homeotropic cell			

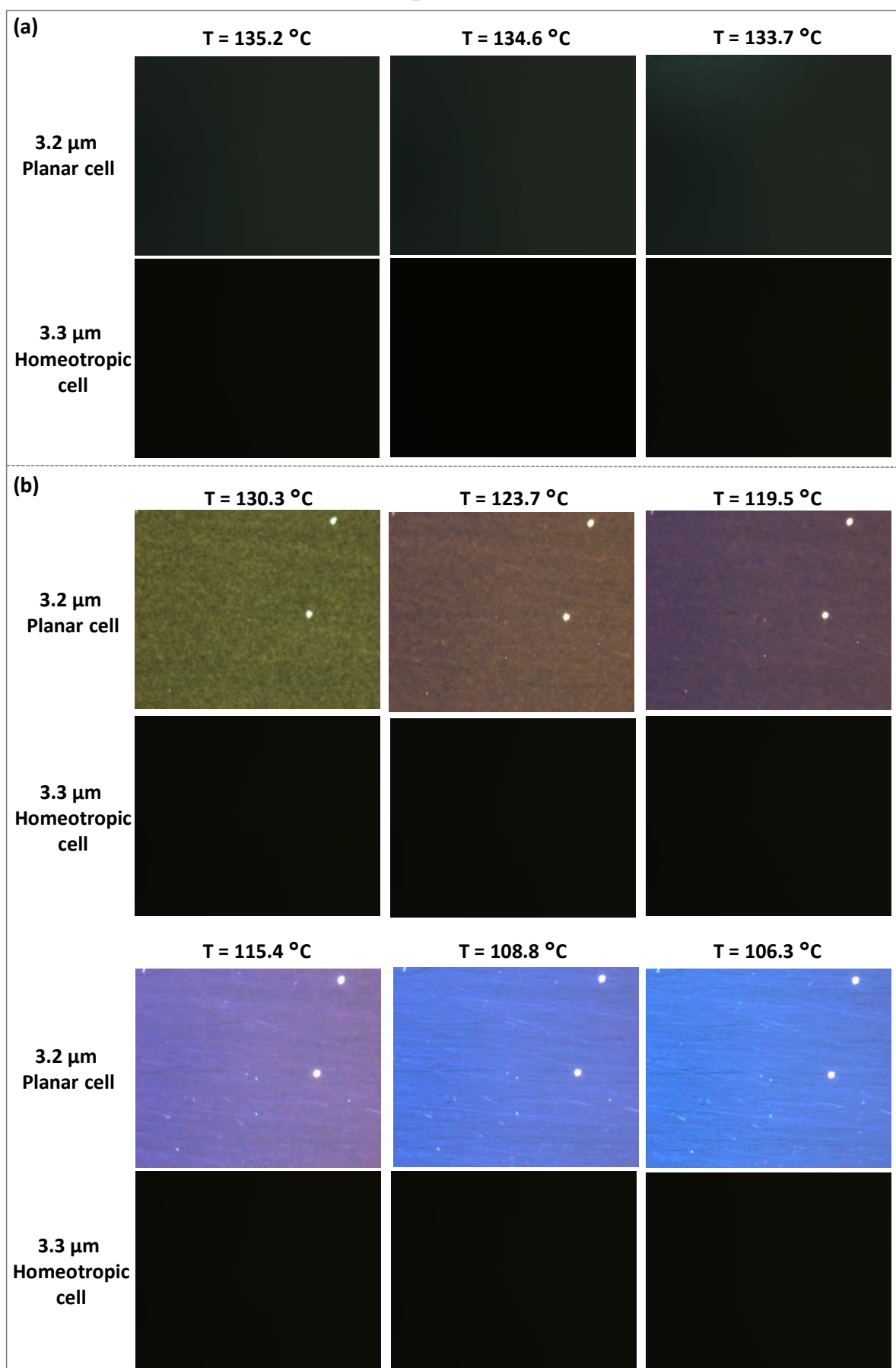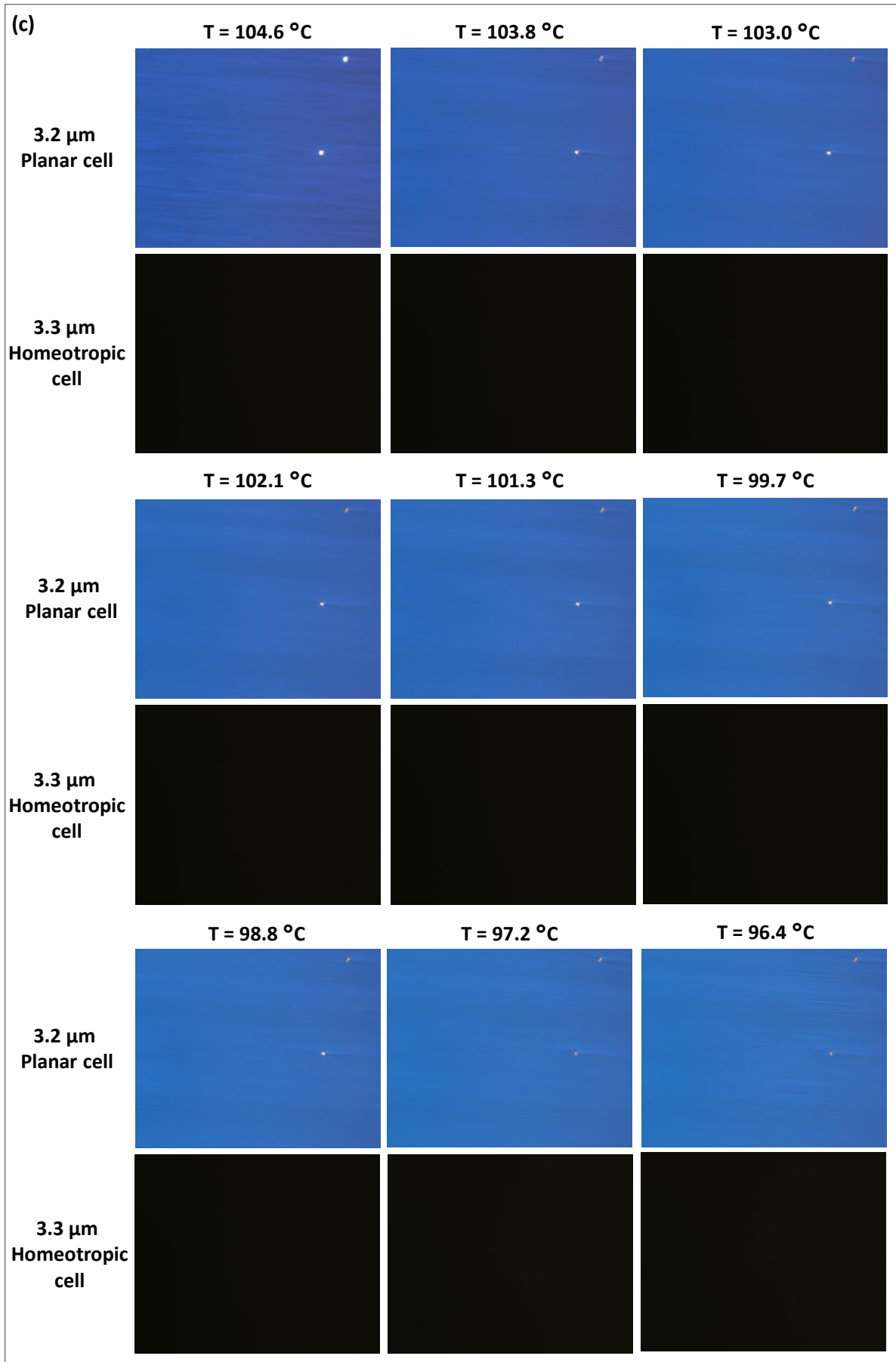|	T = 87.6 °C	T = 86.8 °C	T = 86.0 °C
4.8 μm Planar cell			
3.3 μm Homeotropic cell			

Fig. S18 Optical textures observed by POM for compound **1/10** displaying (a) isotropic, (b) nematic, (c) SmA and (d) SmC phase in the planar (4.8 µm) coated cell and homeotropic (3.3 µm) coated cell (crossed polarizers; X200 magnification).

Compound **1/12**:

(c)

	T = 104.6 °C	T = 103.8 °C	T = 103.0 °C
3.2 μm Planar cell			
3.3 μm Homeotropic cell			

	T = 102.1 °C	T = 101.3 °C	T = 99.7 °C
3.2 μm Planar cell			
3.3 μm Homeotropic cell			

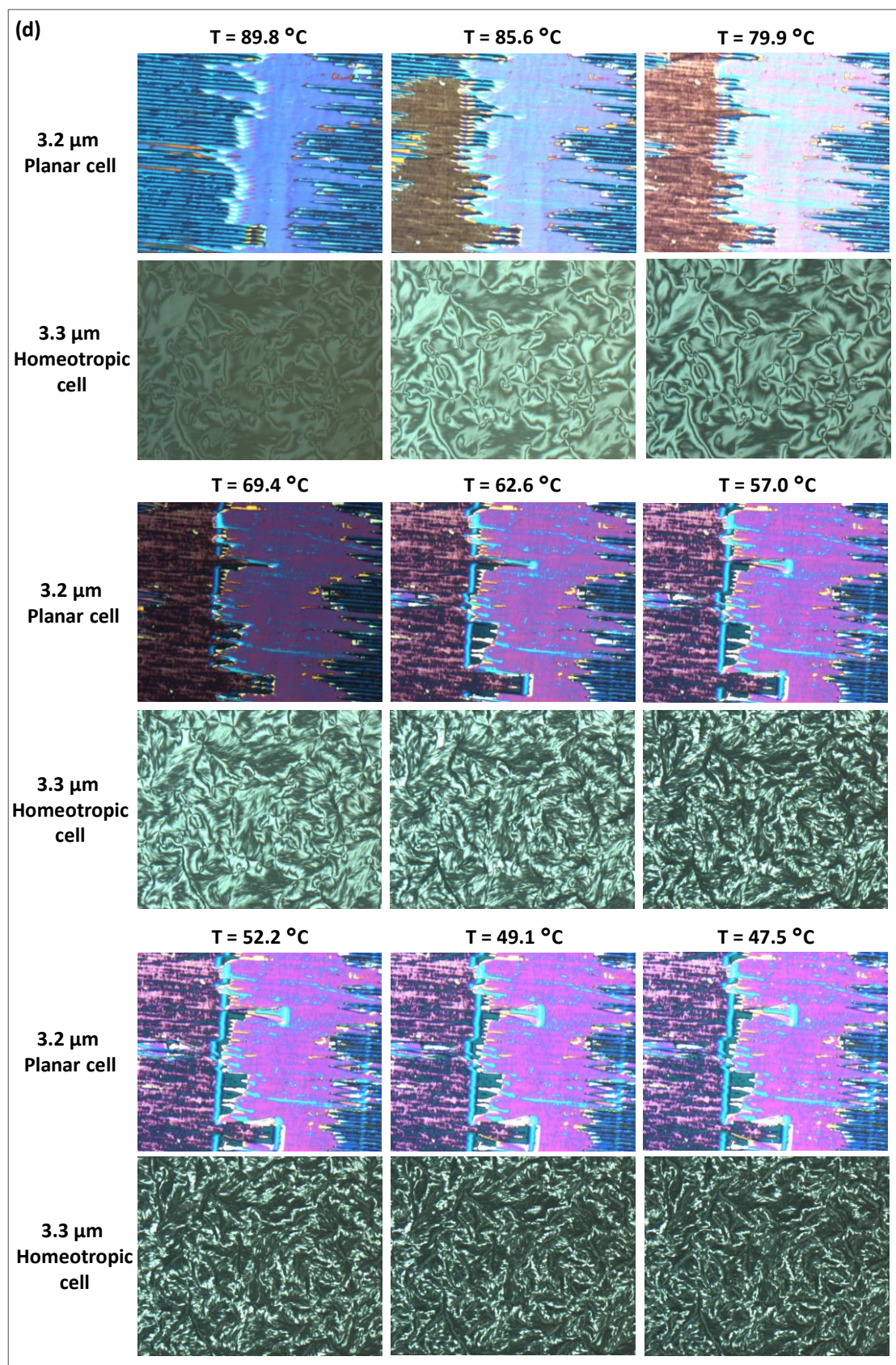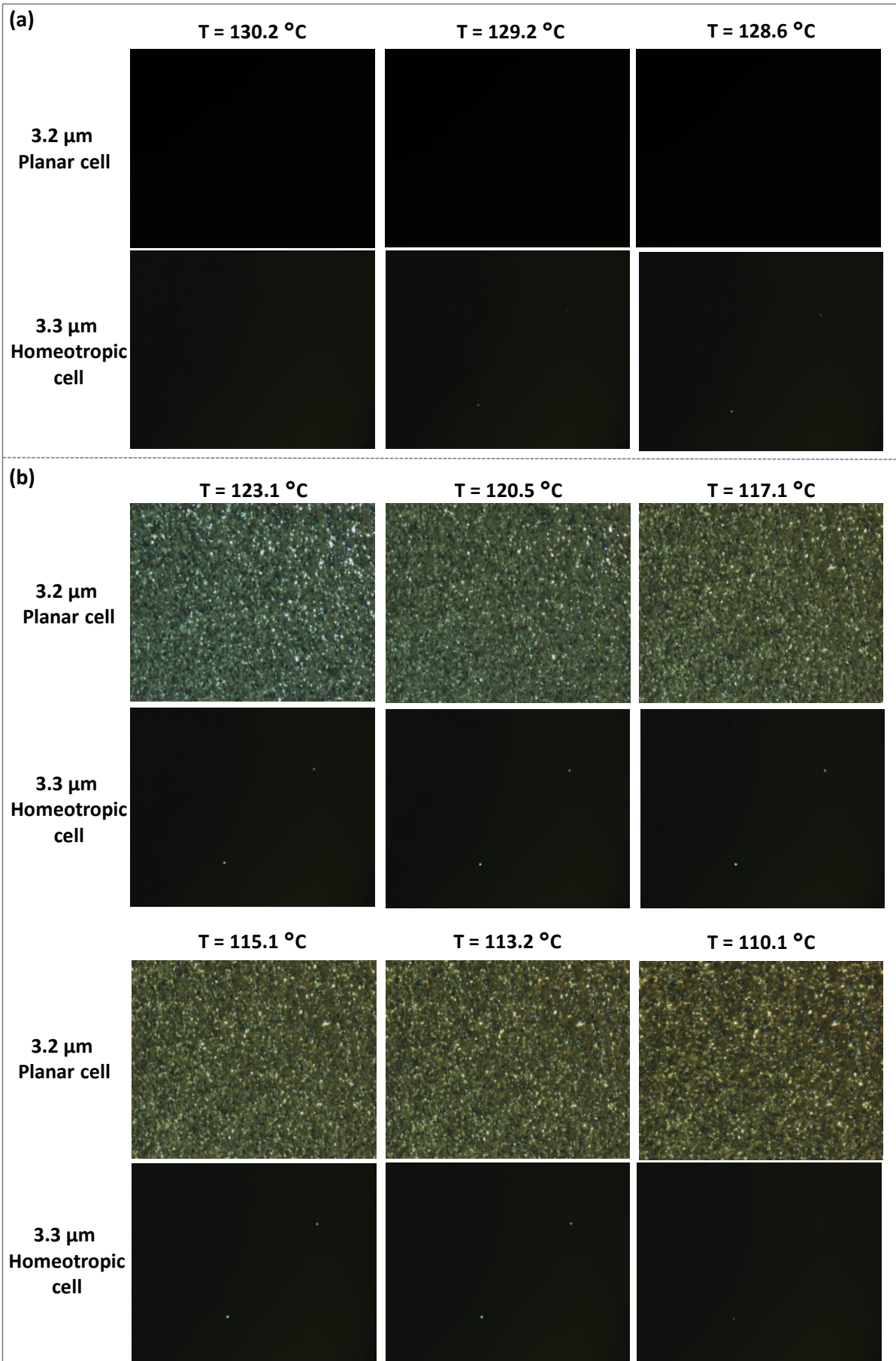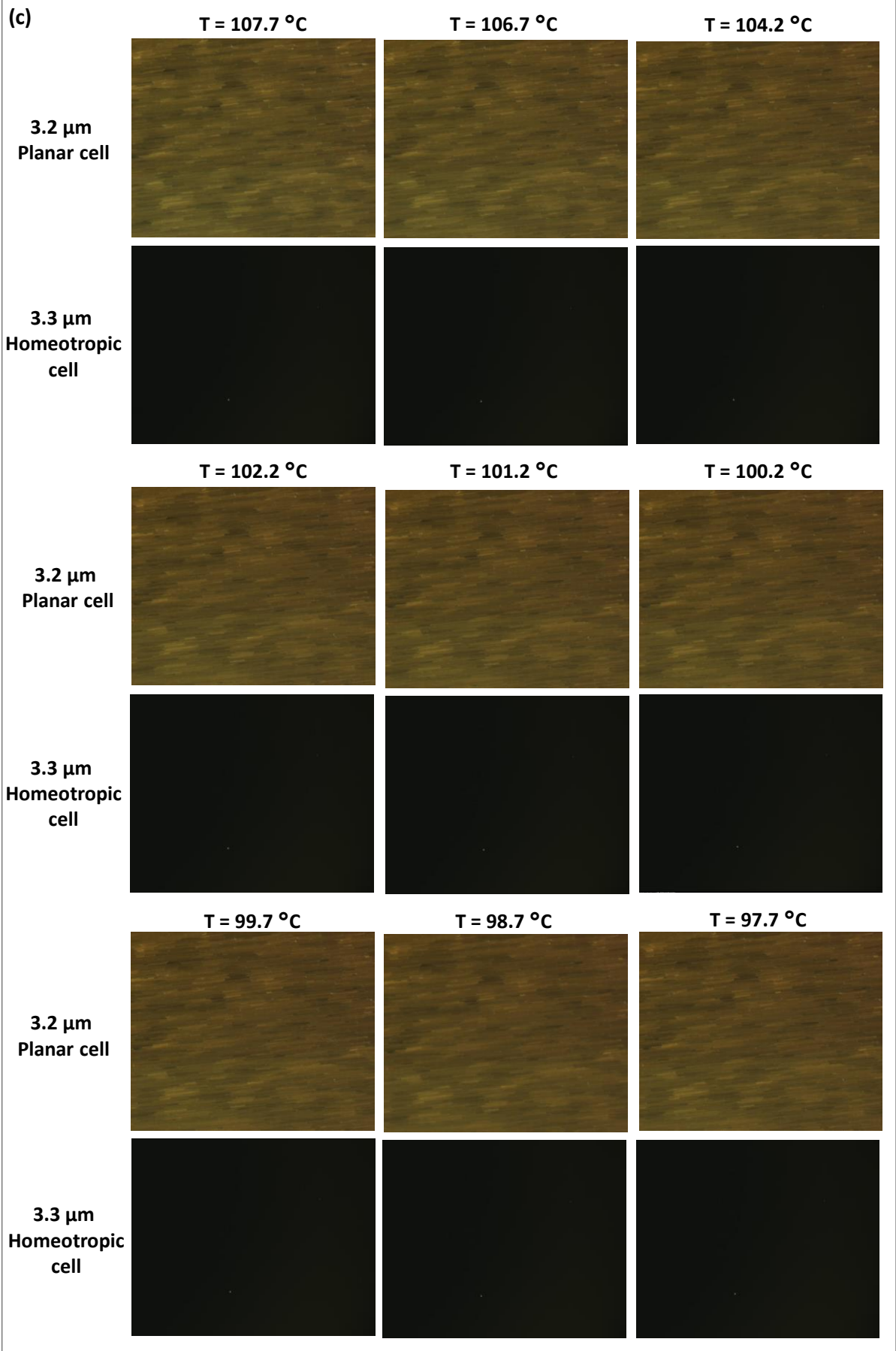|	T = 98.8 °C	T = 97.2 °C	T = 96.4 °C
3.2 μm Planar cell			
3.3 μm Homeotropic cell			

Fig. S19 Optical textures observed by POM for compound **1/12** displaying (a) isotropic, (b) nematic, (c) SmA and (d) SmC phase in the planar (3.2 µm) coated cell and homeotropic (3.3 µm) coated cell (crossed polarizers; X200 magnification).

Compound **1/14**:

In the planar anchoring condition (PI-coated ITO cell with 3.2 µm cell gap), upon cooling from the isotropic phase, compound **1/14** exhibited a birefringent nematic texture at 123.4 °C (Fig. S20b) followed by SmA phase at 108.0 °C (Fig. S20c). Upon further cooling SmA texture converted to a birefringent SmC phase at 84.0 °C (Fig. S20d).

When compound **1/14** was observed under homeotropic anchoring condition (cell gap 3.3 µm with ITO coating and antiparallel rubbing direction), black/dark images were observed for the isotropic, nematic and SmA phases (Fig. S20a, b, c) whereas birefringent schlieren textures were seen for the SmC phase (Fig. S20d).
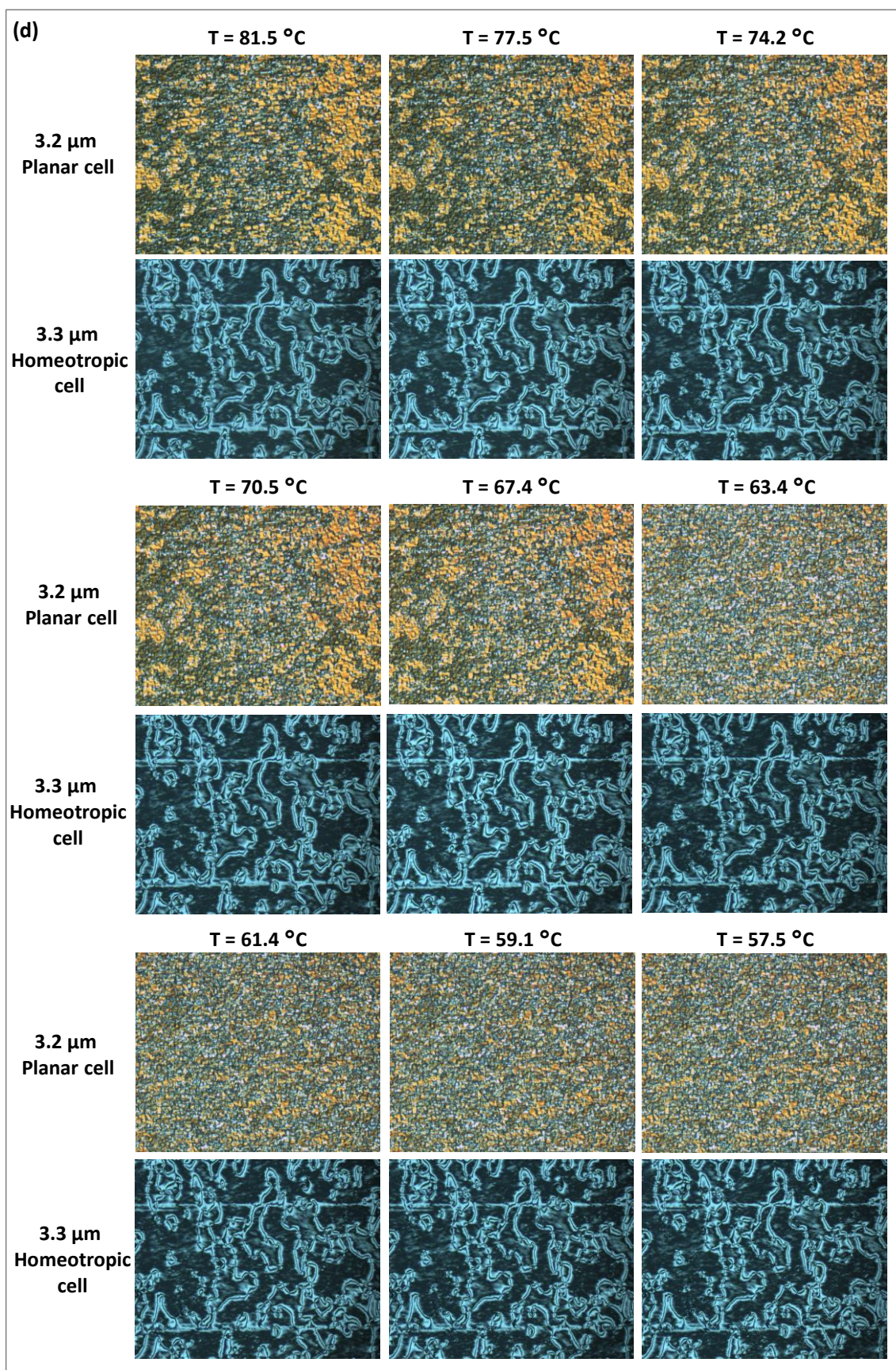
(a)

	T = 130.2 °C	T = 129.2 °C	T = 128.6 °C
3.2 µm Planar cell			
3.3 µm Homeotropic cell			

(b)

	T = 123.1 °C	T = 120.5 °C	T = 117.1 °C
3.2 µm Planar cell			
3.3 µm Homeotropic cell			

	T = 115.1 °C	T = 113.2 °C	T = 110.1 °C
3.2 µm Planar cell			
3.3 µm Homeotropic cell			

(c)

	T = 107.7 °C	T = 106.7 °C	T = 104.2 °C
3.2 µm Planar cell			
3.3 µm Homeotropic cell			

	T = 102.2 °C	T = 101.2 °C	T = 100.2 °C
3.2 µm Planar cell			
3.3 µm Homeotropic cell			

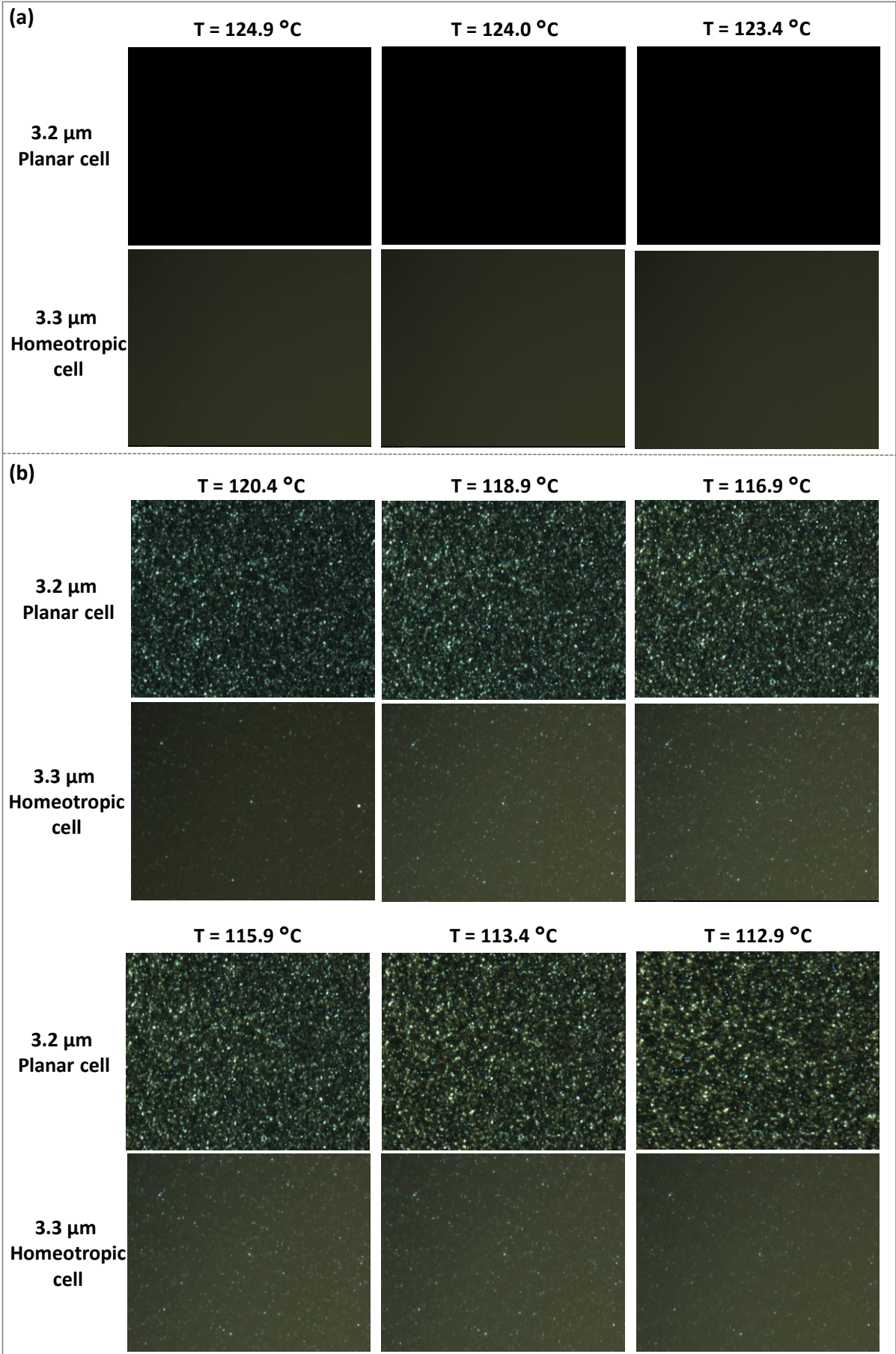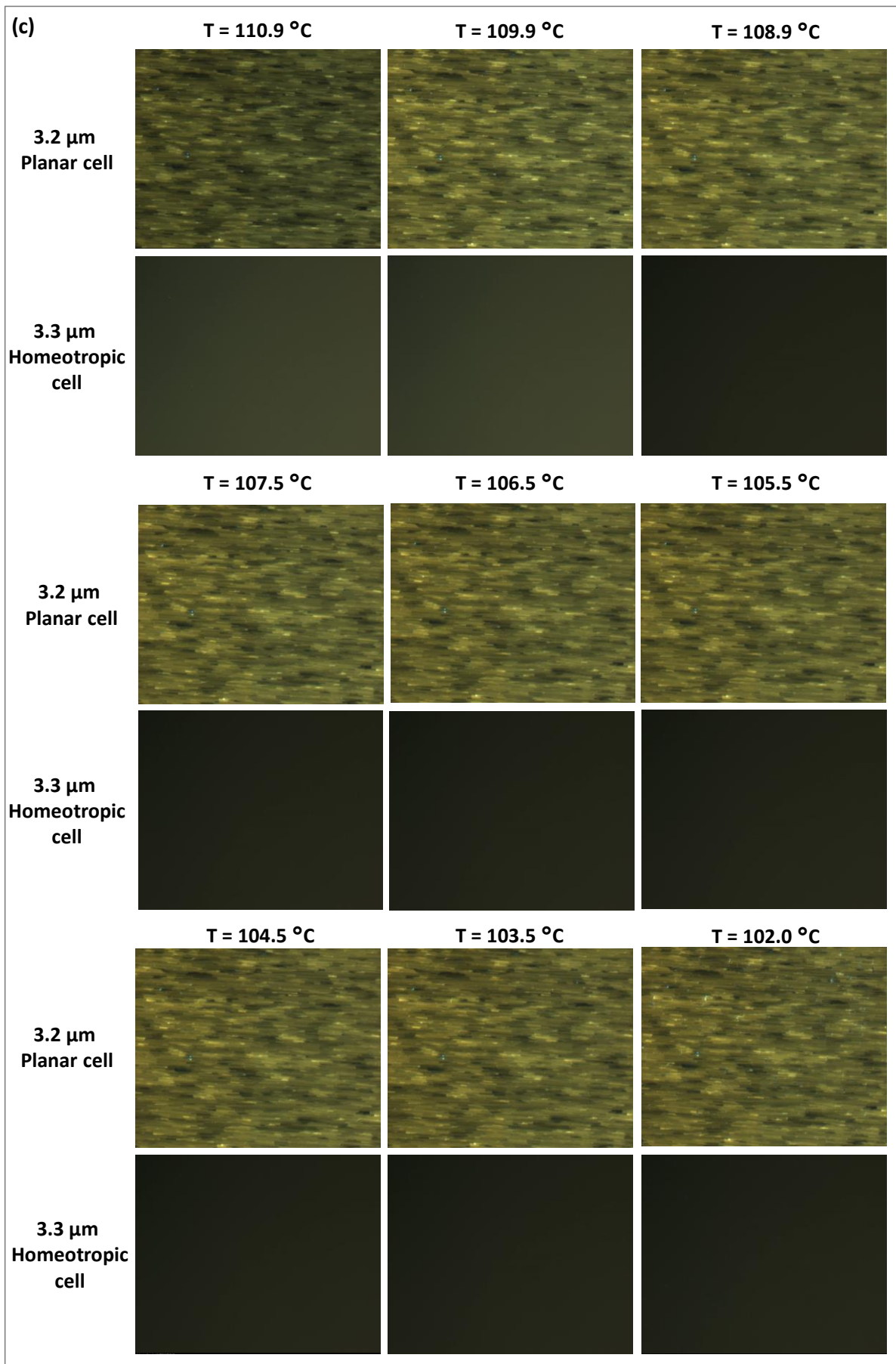|	T = 99.7 °C	T = 98.7 °C	T = 97.7 °C
3.2 µm Planar cell			
3.3 µm Homeotropic cell			

Fig. S20 Optical textures observed by POM for compound **1/14** displaying (a) isotropic, (b) nematic, (c) SmA and (d) SmC phase in the planar (3.2 μm) coated cell and homeotropic (3.3 μm) coated cell (crossed polarizers; X200 magnification).

Compound **1/16**:

In the planar anchoring condition (PI-coated ITO cell with 3.2 µm cell gap), upon cooling from the isotropic phase, compound **1/16** exhibited a birefringent nematic texture at 121.2 °C (Fig. S21b) followed by SmA phase at 111.1 °C (Fig. S21c). Further cooling led to change in the SmA texture to a birefringent SmC phase at 89.0 °C (Fig. S21d).

When compound **1/16** was observed under homeotropic anchoring condition (cell gap 3.3 µm with ITO coating and antiparallel rubbing direction), black/dark images were observed for the isotropic, nematic and SmA phases (Fig. S21a, b, c) but the SmC textures were birefringent (Fig. S21d).
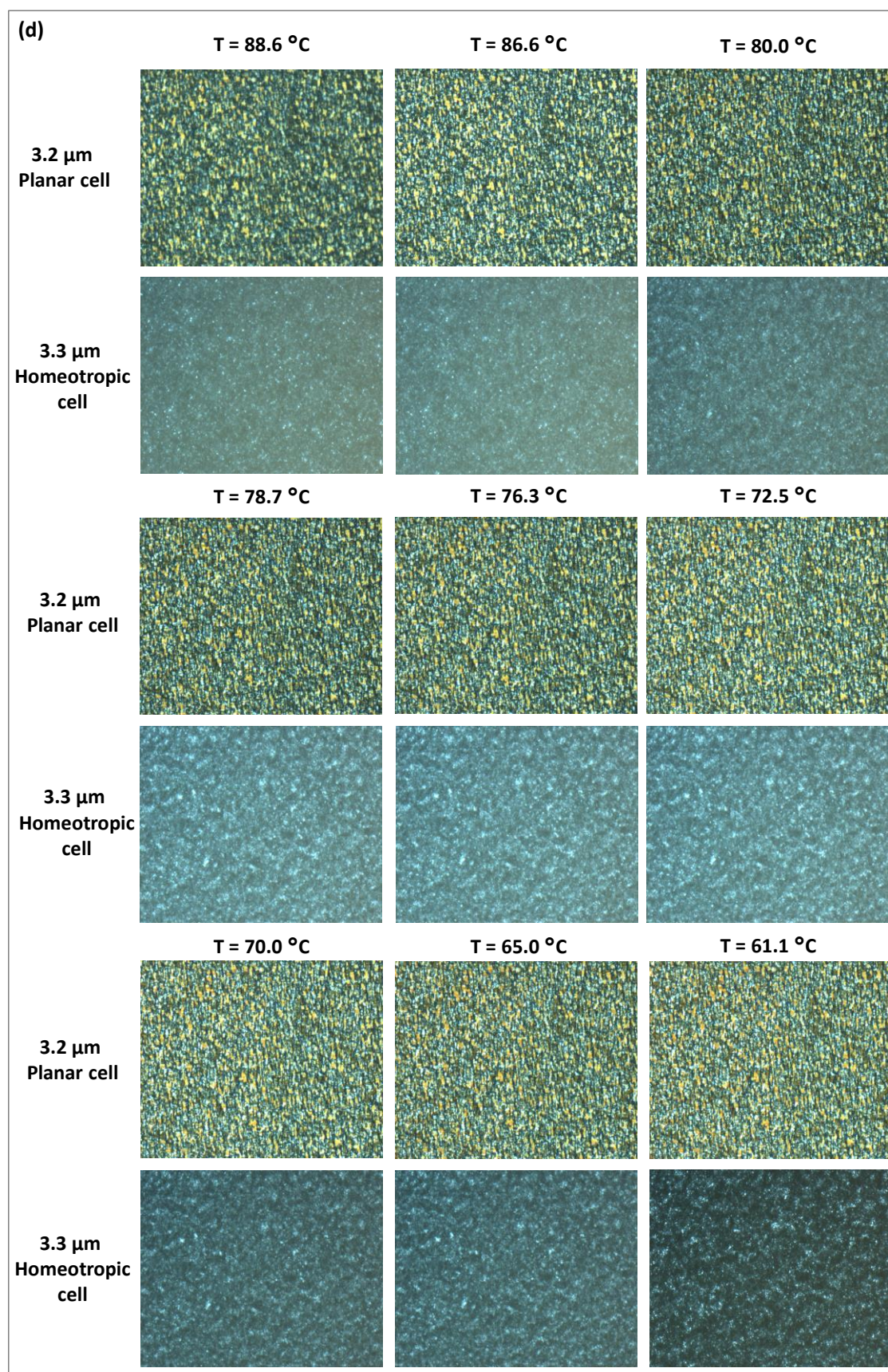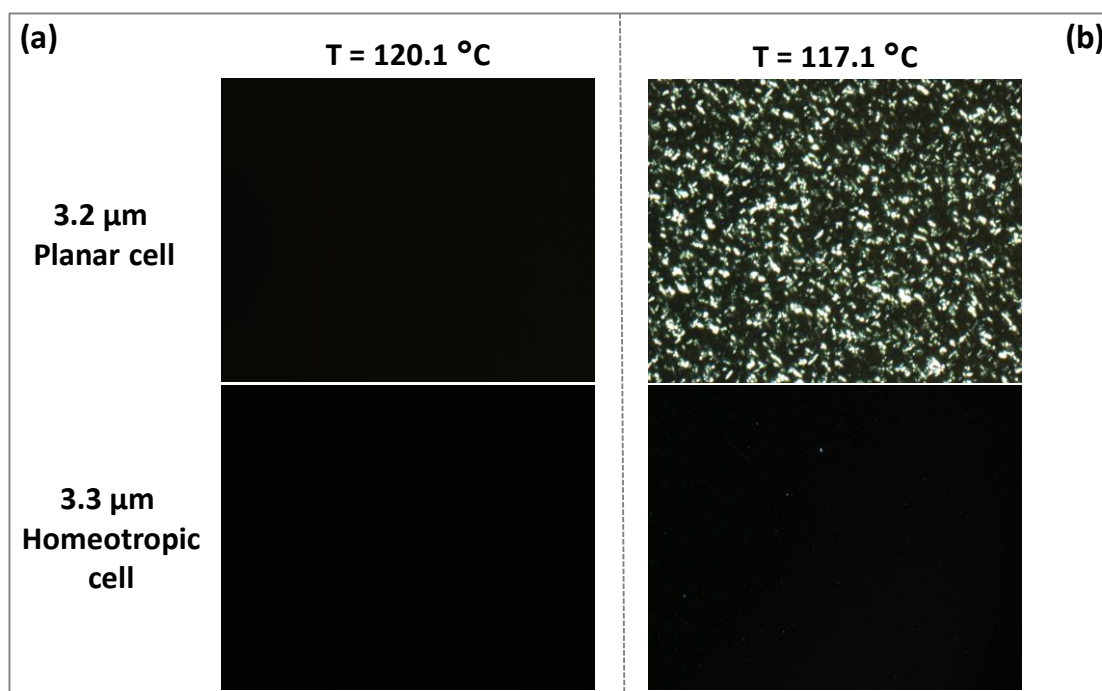
(a)

	T = 124.9 °C	T = 124.0 °C	T = 123.4 °C
3.2 µm Planar cell			
3.3 µm Homeotropic cell			

(b)

	T = 120.4 °C	T = 118.9 °C	T = 116.9 °C
3.2 µm Planar cell			
3.3 µm Homeotropic cell			

	T = 115.9 °C	T = 113.4 °C	T = 112.9 °C
3.2 µm Planar cell			
3.3 µm Homeotropic cell			

(c)

	T = 110.9 °C	T = 109.9 °C	T = 108.9 °C
3.2 µm Planar cell			
3.3 µm Homeotropic cell			

	T = 107.5 °C	T = 106.5 °C	T = 105.5 °C
3.2 µm Planar cell			
3.3 µm Homeotropic cell			

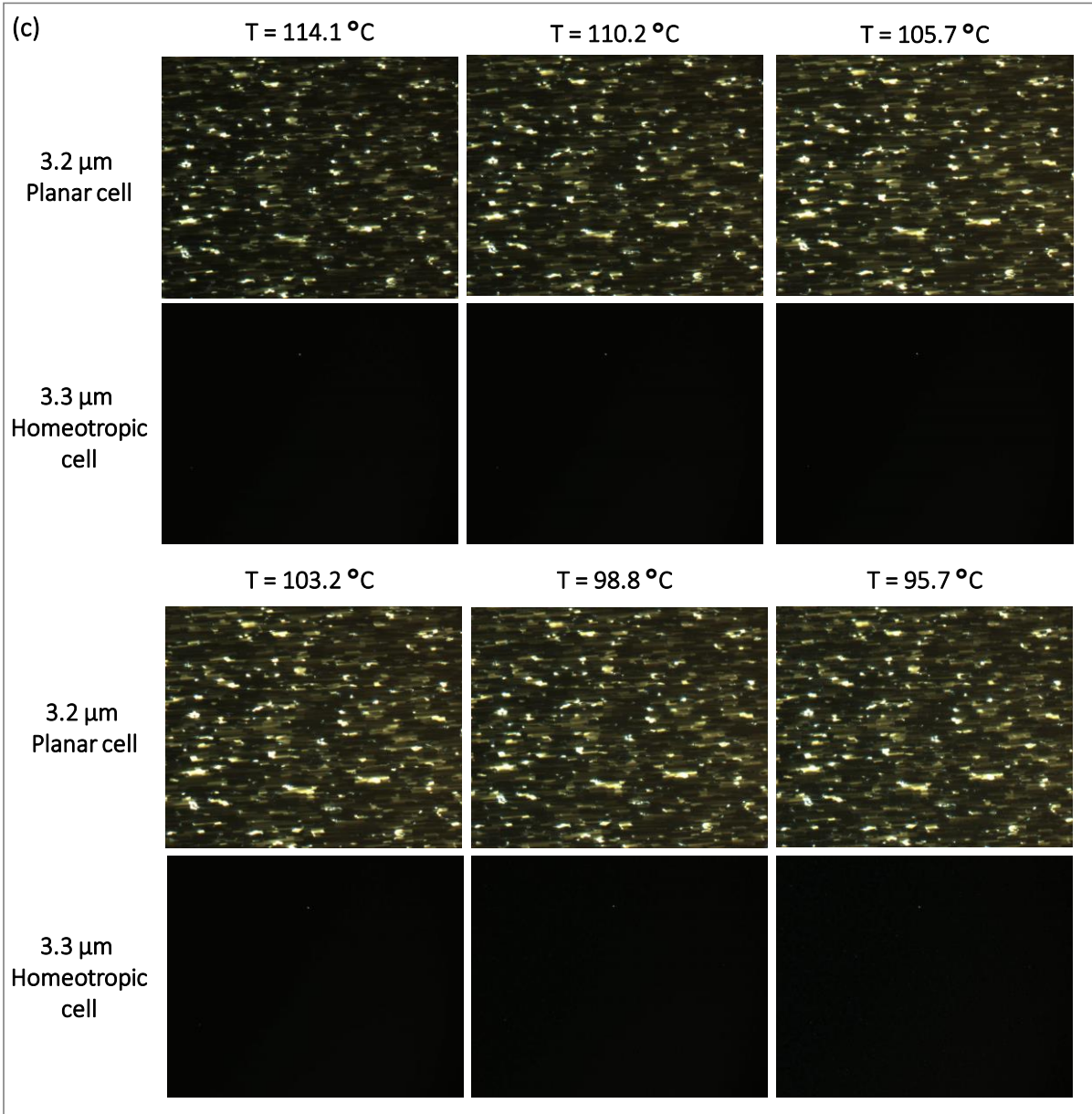|	T = 104.5 °C	T = 103.5 °C	T = 102.0 °C
3.2 µm Planar cell			
3.3 µm Homeotropic cell			

Fig. S21 Optical textures observed by POM for compound **1/16** displaying (a) isotropic, (b) nematic, (c) SmA and (d) SmC phase in the planar (3.2 µm) coated cell and homeotropic (3.3 µm) coated cell (crossed polarizers; X200 magnification).

Compound **1/18**:

Upon cooling from the isotropic phase in planar anchoring cell (PI-coated ITO cell with 3.2 µm cell gap), compound **1/18** converts into a birefringent nematic phase at 117.2 °C (Fig. S22b) and gradually transforms to textures with defects at 114.4 °C corresponding to the SmA phase (Fig. S22c) and gradually to SmC (Fig. S22d) at 94.0 °C. The nature of the smectic mesophases was confirmed with the help of a homeotropic cell (cell gap 3.3 µm with ITO coating and antiparallel rubbing direction). The dark/ black nematic (Fig. S22b) and SmA (Fig. S22c) phases convert to a birefringent texture in homeotropic conditions, implying it to be the SmC phase (Fig. S22d).
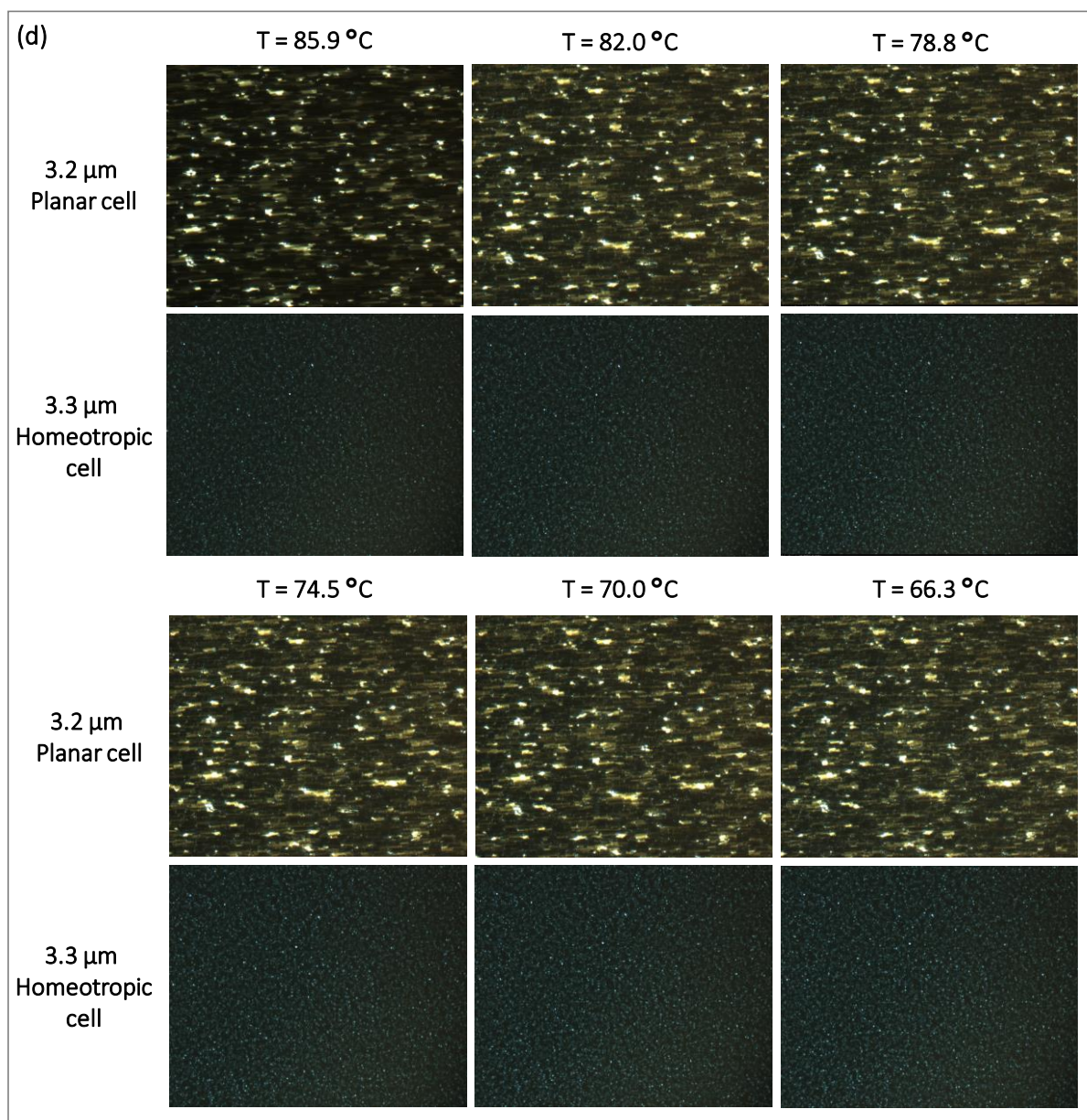
(c)

	T = 114.1 °C	T = 110.2 °C	T = 105.7 °C
3.2 µm Planar cell			
3.3 µm Homeotropic cell			

	T = 103.2 °C	T = 98.8 °C	T = 95.7 °C
3.2 µm Planar cell			
3.3 µm Homeotropic cell			

Fig. S22 Optical textures observed by POM for compound **1/18** displaying (a) isotropic, (b) nematic, (c) SmA and (d) SmC phase in the planar (3.2 µm) coated cell and homeotropic (3.3 µm) coated cell (crossed polarizers; X200 magnification).

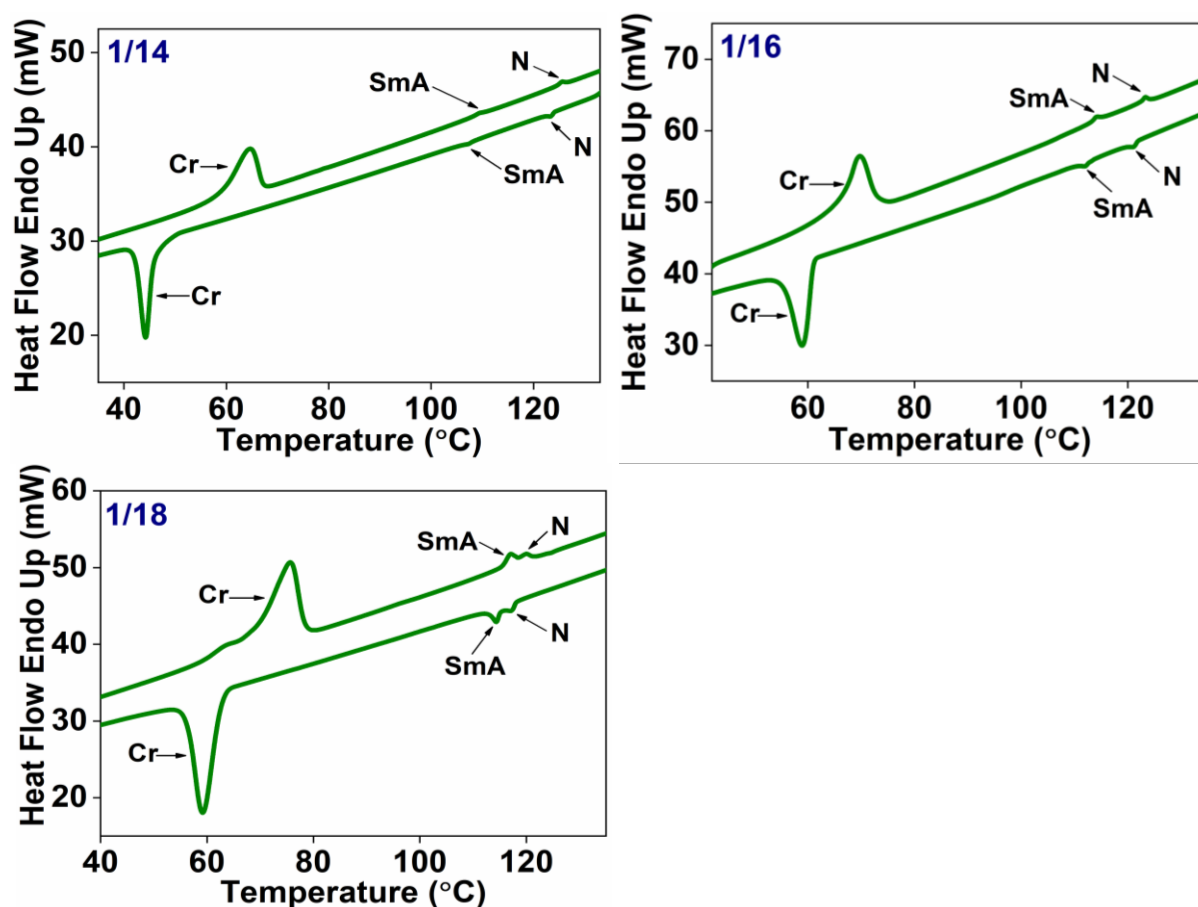## 5. Differential Scanning Calorimetry (DSC) studies:

Fig. S23 DSC thermograms (both heating and cooling cycles) of the final compounds recorded at 10 °C min^{-1}.

6. Structure-property relationship:

- The N-Iso (nematic to isotropic) phase transition temperatures gradually decreased as the length of the alkoxy chain increased (Fig. S24a).
- In the cooling sequence, as the alkoxy chain length increased, nematic phase range decreased whereas the total smectic phase (SmA+SmC) range increased (Fig. S24b).
- In the entire smectic phase regime of a particular compound, SmC phase range was more as compared to SmA (Fig. S24b).
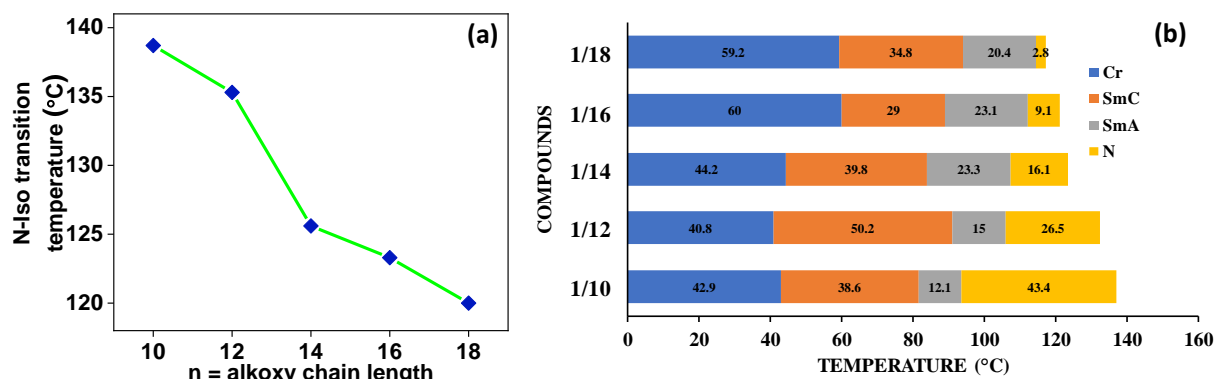
Fig. S24 (a) Variation of terminal alkoxy chain with N-Iso (nematic to isotropic) transition temperature, (b) Bar graph summarizing the thermal behaviour of **1/n** series in the cooling cycle.

7. X-ray Diffraction (XRD) studies:

The layer spacing (d-value) and correlation length (ξ) have been calculated by adopting the method reported earlier.[1,2] The formula and its significance is reproduced below for the convenience of readers:

"**Layer spacing (*d*-value):** The distance between the layers formed in the mesophases.
It was calculated from the Bragg's law,

$$2d \sin\theta = n\lambda$$

where, n is the order of reflection (~1), λ is the wavelength of the incident X-rays, and θ is the angle corresponding to Bragg's reflection.

**Correlation length** (*ξ*)**:** The degree of order of the molecules within the mesophases.
It was calculated by employing the Scherrer's equation,

$$\xi = k\lambda /\Delta 2\theta \cos\theta$$

where, *k* is the shape factor whose typical value is 1, *λ* is the wavelength of the incident X-rays, $\Delta 2\theta$ is the broadening in 2θ at half the maximum intensity (FWHM) in radian unit, and θ is the maximum of the reflection.

Further, the number of correlated units (*ξ/d*) can be calculated by dividing the correlation length (*ξ*) of the peak by corresponding *d*-spacing. It expresses how many units of that length scale are tune in on to show that correlation length."
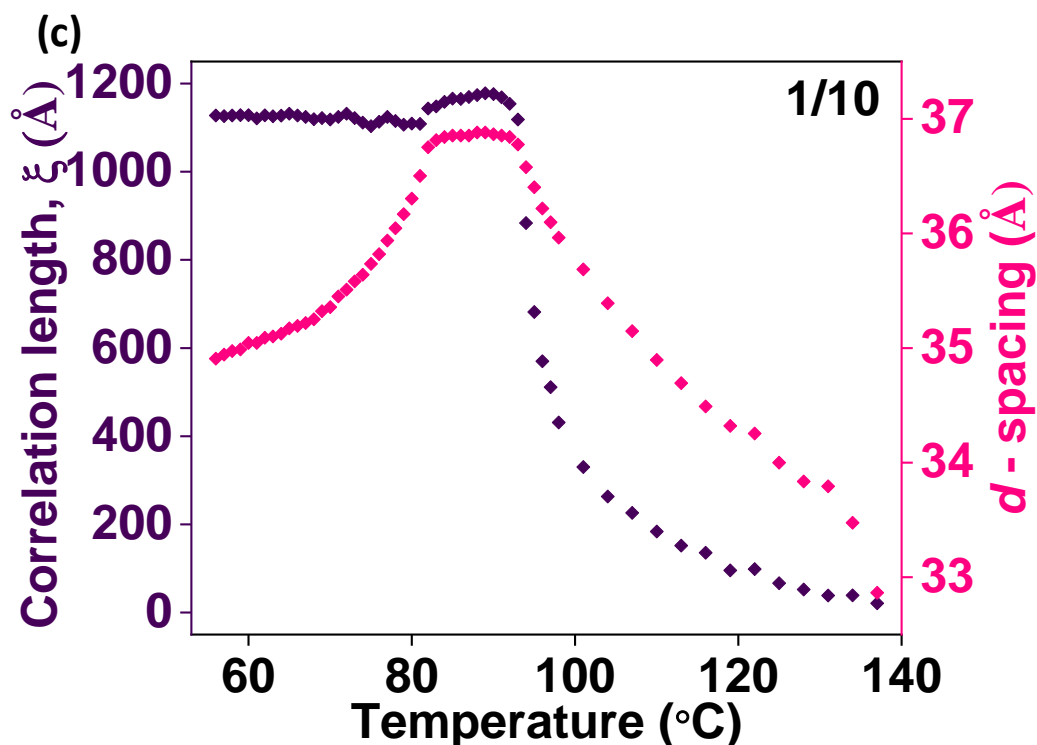
(a) Compound **1/10**:
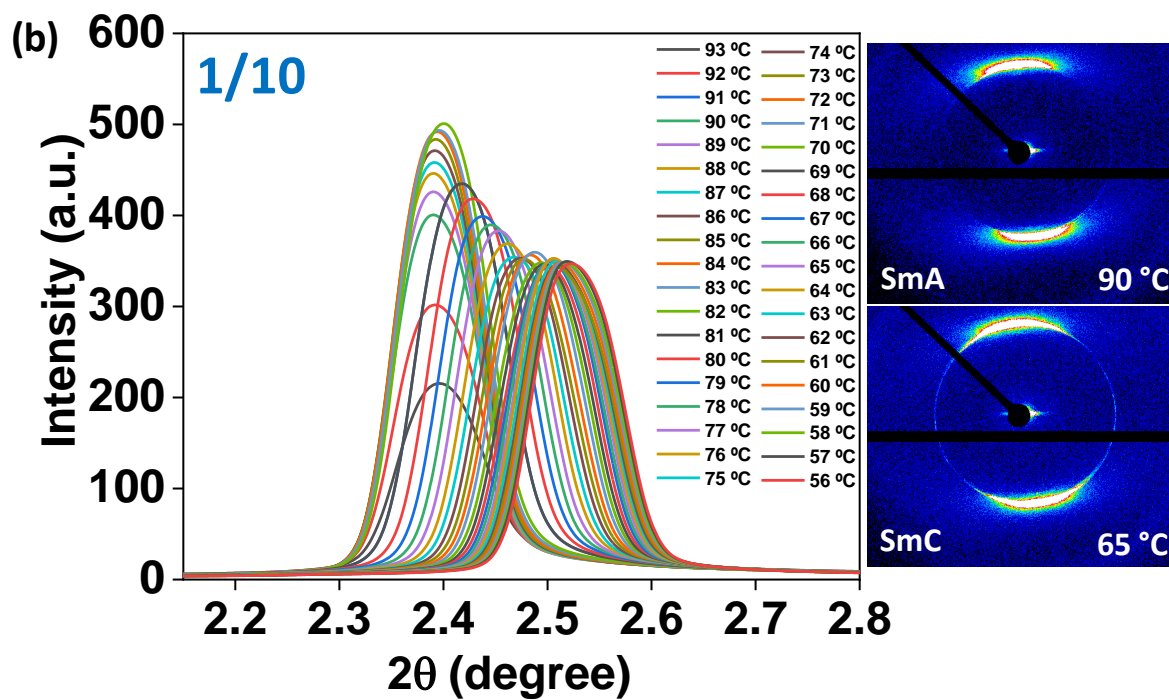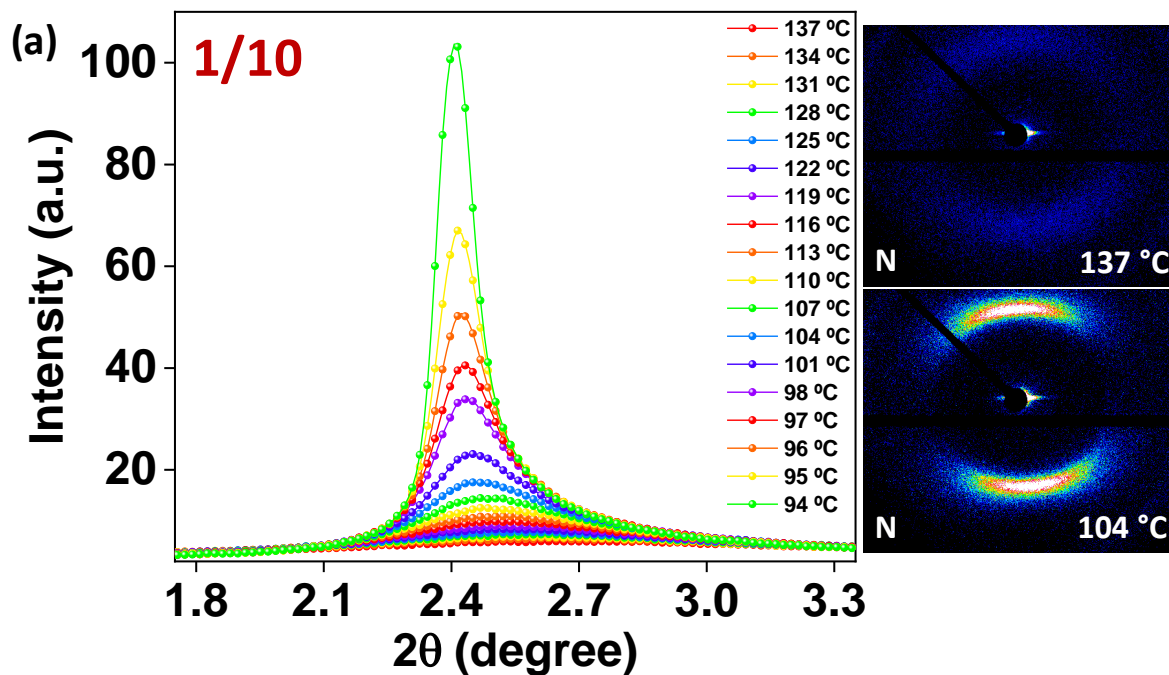
Fig. S25 Intensity (a.u.) *vs.* 2θ (degree) profiles in the small-angle region (SAXS studies) for compound **1/10** in the cooling cycle displaying the (a) Nematic, (b) SmA, SmC phase (the 2D diffraction images are placed on the right). (c) Variation of correlation length (ξ) and *d*-spacing with temperature corresponding to the small angle peak of compound **1/10**.

Table S1. Record of 2θ (°), *d*-spacing (Å), correlation length ξ (Å) and number of correlated units (ξ/*d*) of the mesogens upon decreasing temperature corresponding to the first peak in the small-angle region in the XRD pattern of the compound **1/10**.

Temp (°C)	2θ (°) (small-angle)	*d*-spacing (Å) (small-angle)	ξ (Å)	ξ/*d*	*d*-spacing (Å) (wide-angle)
134 (N)	2.64	33.48	38.87	1.16	5.05
131	2.61	33.79	38.66	1.14	
128	2.60	33.84	52.02	1.54	
125	2.60	34.00	66.47	1.95	
122	2.58	34.25	98.44	2.87	
119	2.57	34.32	95.47	2.78	
116	2.56	34.49	135.74	3.94	
113	2.54	34.69	151.76	4.37	
110	2.53	34.90	183.80	5.27	
107	2.51	35.15	226.20	6.43	
104	2.49	35.39	263.26	7.44	
101	2.47	35.69	330.21	9.25	
98	2.45	35.96	431.06	11.99	

97	2.44	36.10	511.09	14.16	
96	2.44	36.22	569.87	15.73	
95	2.42	36.40	681.82	18.73	
94	2.41	36.58	883.43	24.15	
93 (SmA)	2.40	36.78	1118.57	30.42	4.92
92	2.40	36.84	1153.96	31.32	
91	2.39	36.85	1168.63	31.70	
90	2.39	36.87	1175.95	31.90	
89	2.39	36.88	1177.99	31.94	
88	2.39	36.88	1174.07	31.83	
87	2.39	36.85	1169.56	31.74	
86	2.39	36.85	1165.08	31.62	
85	2.39	36.85	1166.00	31.64	
84	2.40	36.84	1158.66	31.45	
83	2.40	36.81	1148.25	31.19	
82	2.40	36.75	1143.49	31.11	
81 (SmC)	2.42	36.50	1108.45	30.37	4.90
80	2.43	36.30	1109.29	30.56	
79	2.44	36.17	1106.65	30.60	
78	2.45	36.05	1115.18	30.94	
77	2.46	35.94	1124.28	31.28	
76	2.46	35.82	1113.22	31.08	
75	2.47	35.73	1103.20	30.87	
74	2.48	35.64	1111.40	31.18	
73	2.48	35.58	1121.85	31.53	
72	2.49	35.50	1131.78	31.87	
71	2.49	35.45	1124.14	31.70	
70	2.50	35.36	1118.44	31.63	
69	2.50	35.32	1121.57	31.75	
68	2.50	35.25	1119.01	31.74	
67	2.50	35.22	1124.29	31.92	
66	2.50	35.19	1127.74	32.04	
65	2.50	35.17	1131.79	32.18	
64	2.51	35.12	1127.30	32.09	
63	2.51	35.10	1125.72	32.07	
62	2.51	35.09	1127.88	32.14	
61	2.52	35.04	1120.86	31.98	
60	2.52	35.04	1128.17	32.19	
59	2.52	34.99	1128.32	32.25	
58	2.52	34.97	1127.74	32.24	
57	2.53	34.94	1126.16	32.23	
56	2.53	34.90	1127.74	32.30	

The correlation length (ξ) and layer spacing (d-value) increased upon cooling from N to SmA phase and remained almost constant in the SmA phase regime. Both these parameters gradually decreased upon transition from SmA to SmC phase. The number of correlated units were similar in both the SmA and SmC phases (30-32 units); where ξ/d value first gradually decreased in the SmA phase range and then increased in the SmC phase in the cooling cycle.

Layer shrinkage:

d_A (82 ˚C) = 36.75 Å, d_C (81 ˚C) = 36.50 Å

Layer shrinkage = [(d_A-d_C) / d_A] * 100 = **0.68 %**
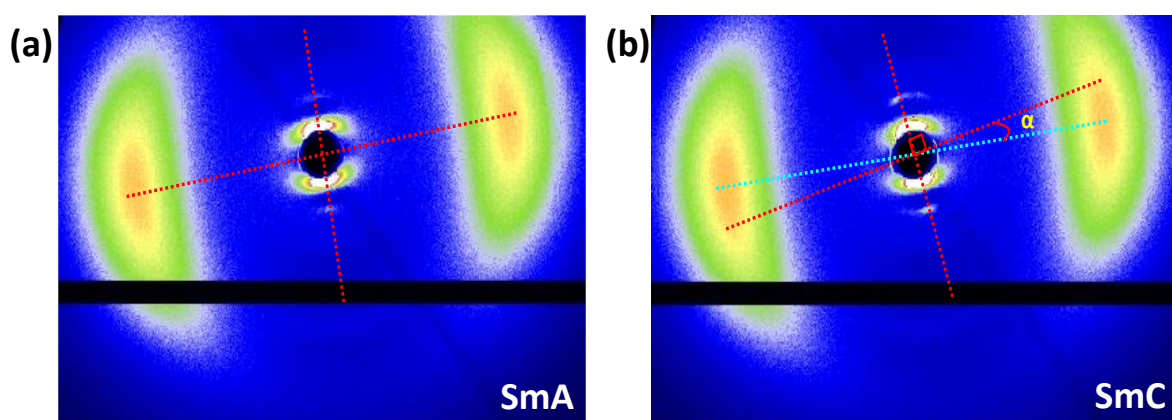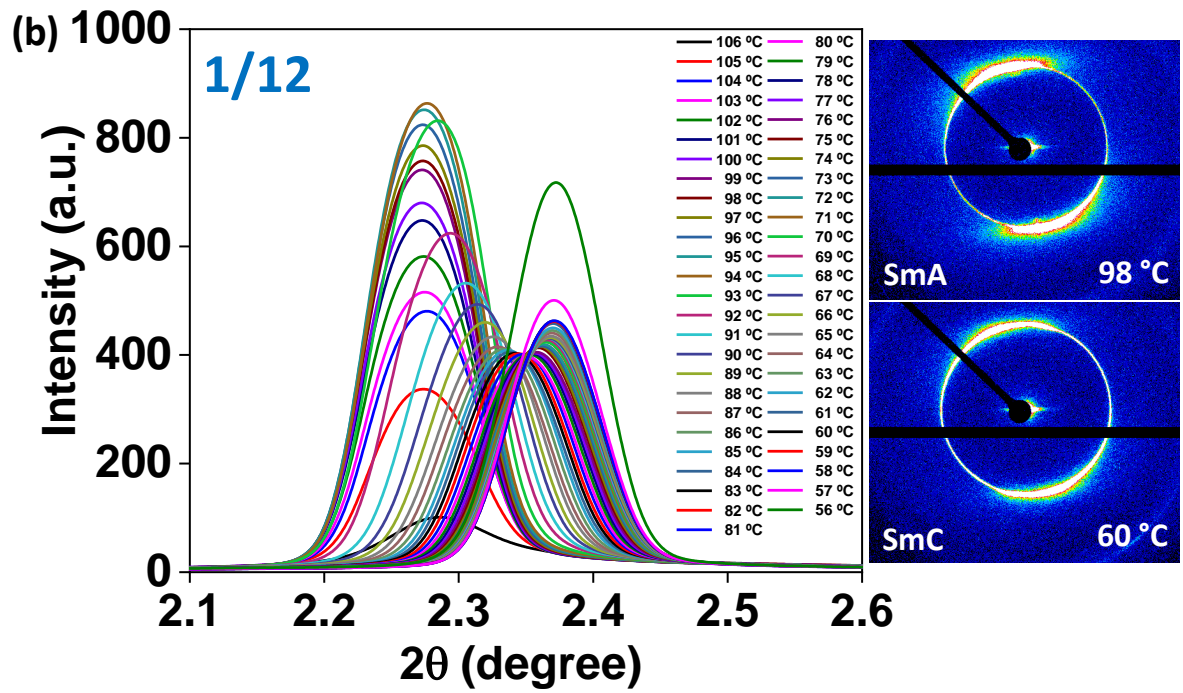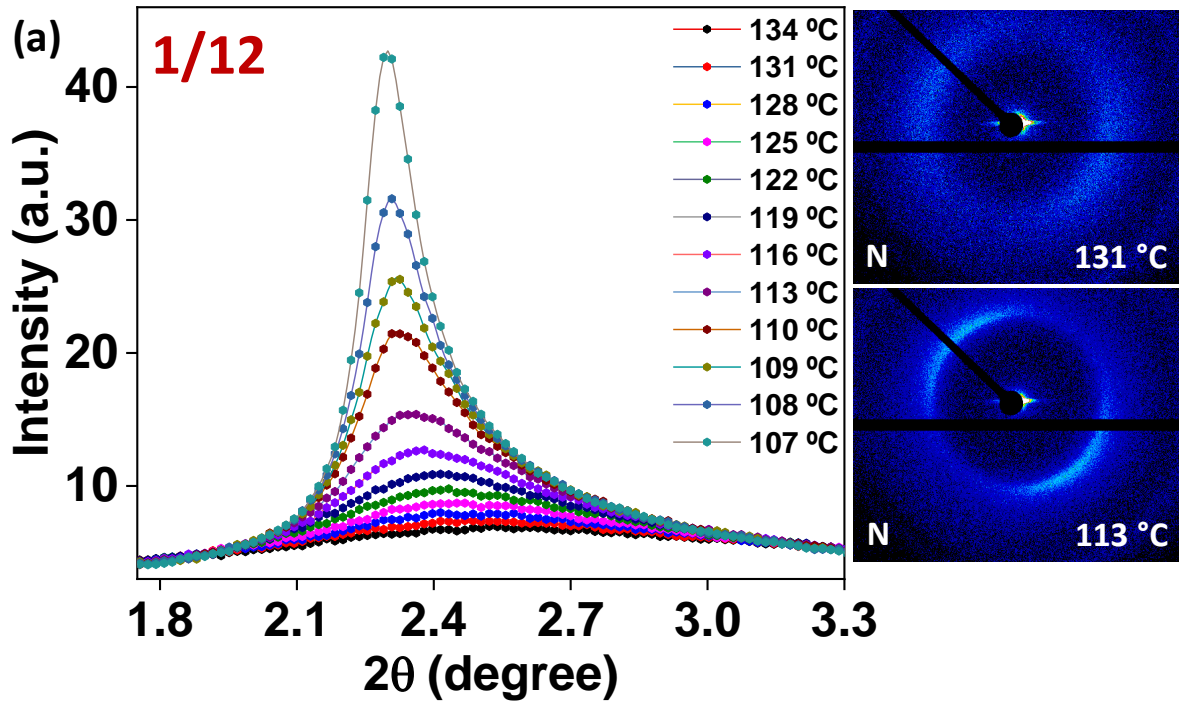

Fig. S26 (a,b) 2D X-ray diffraction patterns for compound **1/10** illustrating a change in the molecular tilt from SmA-SmC phase transition.
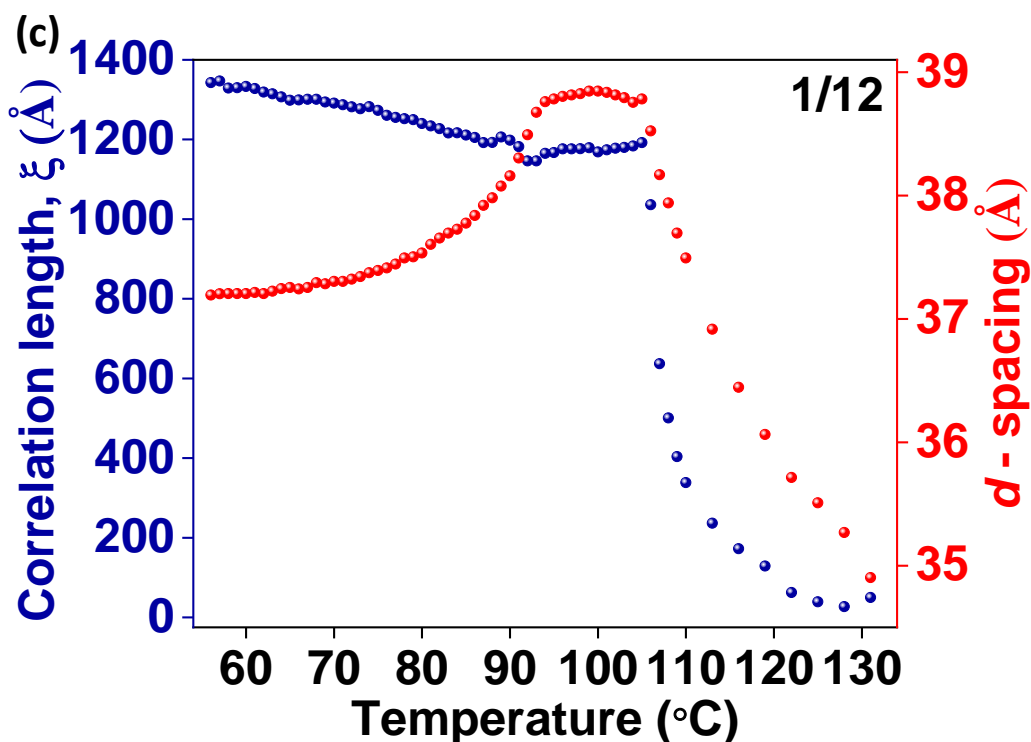
(b) Compound **1/12**:

Fig. S27 Intensity (a.u.) *vs.* 2θ (degree) profiles in the small-angle region (SAXS studies) for compound **1/12** in the cooling cycle displaying the (a) Nematic, (b) SmA, SmC phase (the 2D diffraction images are placed on the right). (c) Variation of correlation length (ξ) and *d*-spacing with temperature corresponding to the small angle peak of compound **1/12**.

Table S2. Record of 2θ (°), *d*-spacing (Å), correlation length ξ (Å) and number of correlated units (ξ/d) of the mesogens upon decreasing temperature corresponding to the first peak in the small-angle region in the XRD pattern of the compound **1/12**.

Temp (°C)	2θ (°) (small-angle)	*d*-spacing (Å) (small-angle)	ξ (Å)	ξ/d	*d*-spacing (Å) (wide-angle)
131 (N)	2.53	34.90	50.04	1.43	5.09
125	2.49	35.50	39.25	1.10	
122	2.47	35.71	62.46	1.75	
119	2.45	36.06	128.79	3.57	
116	2.42	36.45	172.35	4.73	
113	2.39	36.92	236.35	6.40	
110	2.35	37.49	338.46	9.02	
109	2.34	37.70	403.78	10.71	
108	2.32	37.94	500.96	13.20	
107	2.31	38.17	637.07	16.69	
106 (SmA)	2.29	38.52	1036.08	26.89	5.01
105	2.28	38.78	1191.96	30.73	
104	2.28	38.76	1183.49	30.54	
103	2.28	38.79	1179.85	30.41	

102	2.27	38.82	1178.12	30.35	
101	2.27	38.84	1173.89	30.23	
100	2.27	38.85	1168.76	30.09	
99	2.27	38.85	1179.22	30.36	
98	2.27	38.83	1176.70	30.30	
97	2.27	38.82	1176.54	30.31	
96	2.27	38.80	1176.23	30.31	
95	2.28	38.78	1167.21	30.10	
94	2.28	38.76	1165.06	30.06	
93	2.28	38.67	1146.14	29.63	
92	2.29	38.49	1146.00	29.77	
91 (SmC)	2.30	38.30	1182.07	30.86	4.97
90	2.31	38.16	1198.28	31.40	
89	2.32	38.08	1206.14	31.68	
88	2.32	37.98	1192.46	31.40	
87	2.33	37.92	1192.30	31.44	
86	2.33	37.84	1204.83	31.84	
85	2.34	37.78	1211.11	32.06	
84	2.34	37.73	1216.79	32.25	
83	2.34	37.70	1216.12	32.26	
82	2.34	37.65	1227.28	32.59	
81	2.35	37.60	1234.15	32.82	
80	2.35	37.53	1240.22	33.04	
79	2.35	37.50	1249.88	33.32	
78	2.35	37.49	1252.00	33.39	
77	2.36	37.44	1255.39	33.53	
76	2.36	37.41	1260.41	33.69	
75	2.36	37.39	1273.14	34.05	
74	2.36	37.37	1282.20	34.30	
73	2.36	37.34	1277.20	34.20	
72	2.36	37.32	1282.02	34.35	
71	2.37	37.30	1287.26	34.50	
70	2.37	37.30	1291.40	34.62	
69	2.37	37.29	1294.24	34.71	
68	2.37	37.29	1300.92	34.88	
67	2.37	37.25	1300.92	34.92	
66	2.37	37.24	1299.20	34.88	
65	2.37	37.25	1298.43	34.85	
64	2.37	37.24	1307.08	35.09	
63	2.37	37.22	1314.48	35.31	
62	2.37	37.20	1319.00	35.45	
61	2.37	37.21	1327.93	35.68	
60	2.37	37.20	1332.95	35.82	

59	2.37	37.20	1329.93	35.75
58	2.37	37.20	1329.13	35.725
57	2.37	37.20	1346.98	36.20
56	2.37	37.19	1342.89	36.10

N to SmA phase transition in **1/12**: The correlation length (ξ) and layer spacing (d-value) increased and as a result ξ/d value increased.

SmA to SmC phase transition in **1/12**: The layer spacing (d-value) decreased but correlation length (ξ) increased which resulted in an increased ξ/d value.

Layer shrinkage:

d_A (92 ˚C) = 38.49 Å, d_C (91 ˚C) = 38.30 Å

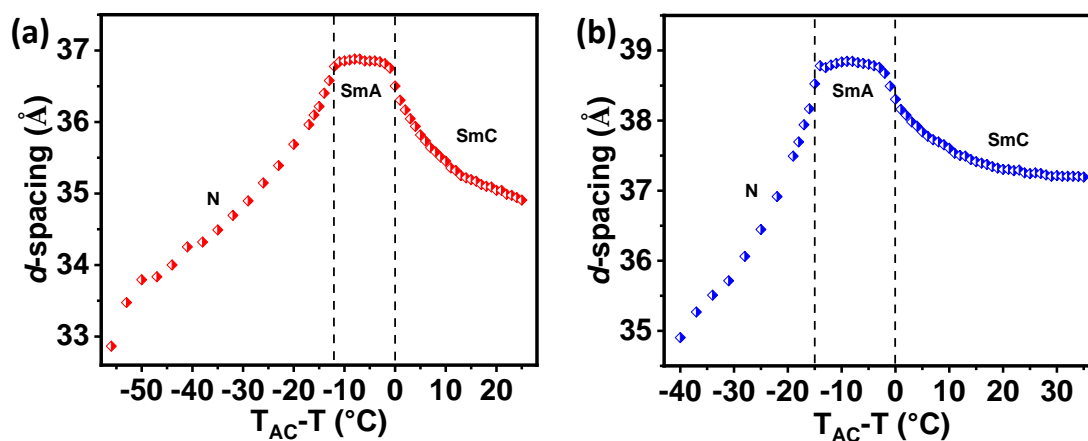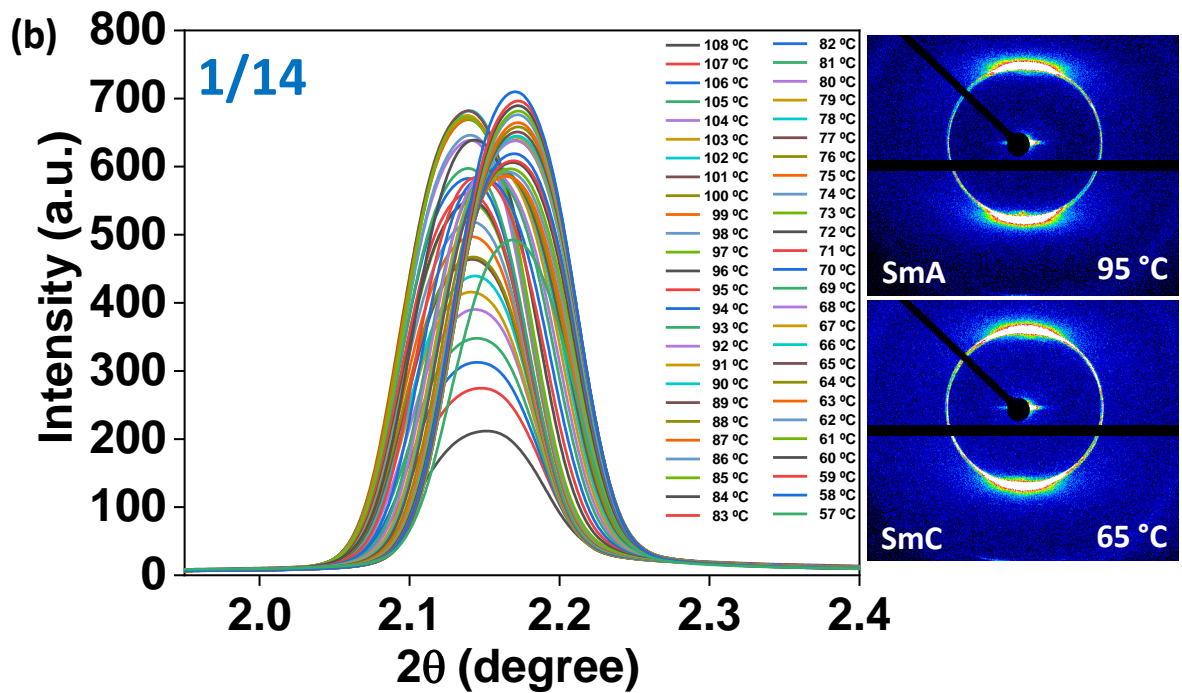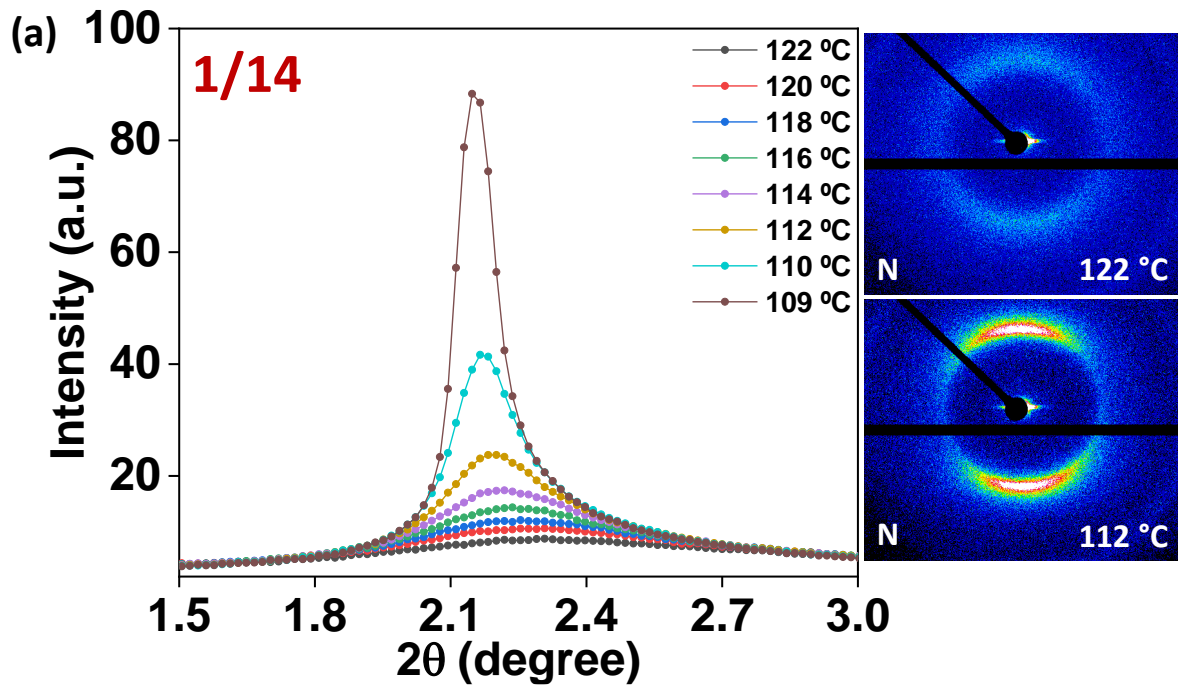Layer shrinkage = [(d_A-d_C) / d_A] * 100 = **0.49 %**

Fig. S28 Variation of d-spacing in various phases with temperature for compounds: (a) **1/10** and (b) **1/12**.
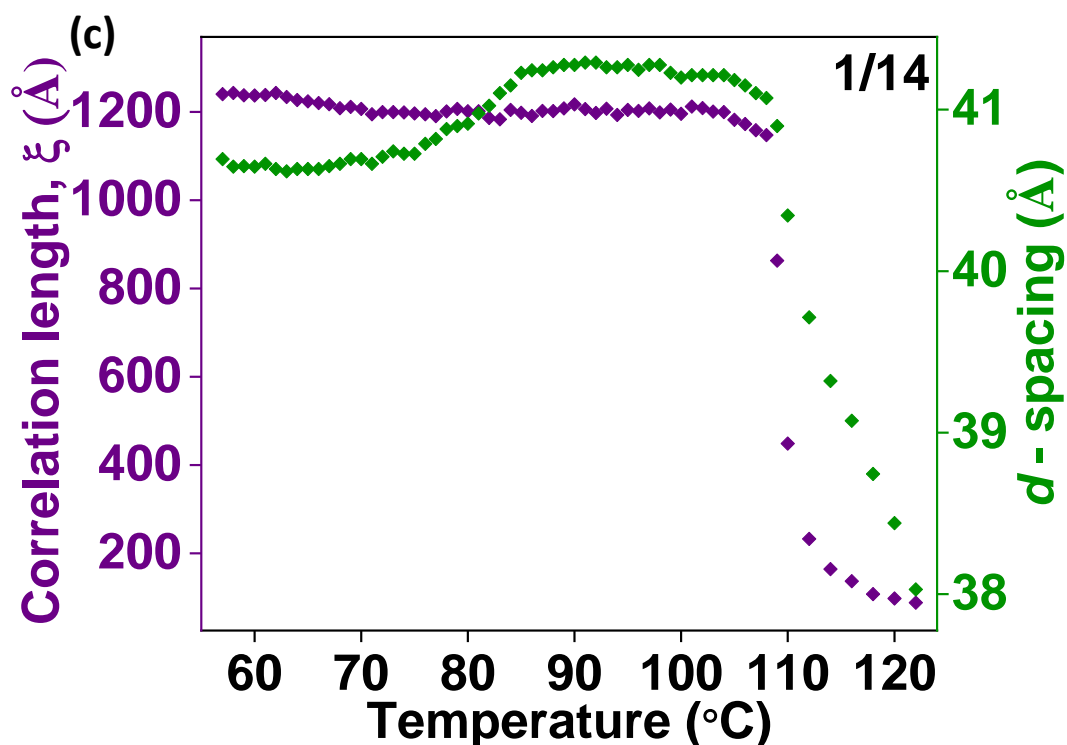
(c) Compound **1/14**:

Fig. S29 Intensity (a.u.) *vs.* 2θ (degree) profiles in the small-angle region (SAXS studies) for compound **1/14** in the cooling cycle displaying the (a) Nematic, (b) SmA, SmC phase (the 2D diffraction images are placed on the right). (c) Variation of correlation length (ξ) and *d*-spacing with temperature corresponding to the small angle peak of compound **1/14**.

Table S3. Record of 2θ (°), *d*-spacing (Å), correlation length ξ (Å) and number of correlated units (ξ/*d*) of the mesogens upon decreasing temperature corresponding to the first peak in the small-angle region in the XRD pattern of the compound **1/14**.

Temp (°C)	2θ (°) (small-angle)	*d*-spacing (Å) (small-angle)	ξ (Å)	ξ/*d*	*d*-spacing (Å) (wide-angle)
122 (N)	2.32	38.03	88.03	2.3	5.05
120	2.30	38.44	97.62	2.54	
118	2.28	38.75	107.42	2.78	
116	2.26	39.07	136.64	3.50	
114	2.24	39.32	164.26	4.20	
112	2.22	39.71	232.71	5.86	
110	2.19	40.34	448.78	11.12	
109	2.16	40.90	863.26	21.10	
108 (SmA)	2.15	41.07	1147.46	27.94	4.98
107	2.15	41.10	1158.45	28.19	
106	2.14	41.15	1172.61	28.50	
105	2.14	41.18	1182.20	28.70	
104	2.14	41.21	1199.71	29.11	
103	2.14	41.21	1200.86	29.14	

102	2.14	41.21	1208.59	29.32	
101	2.14	41.21	1212.07	29.40	
100	2.14	41.20	1195.97	29.03	
99	2.14	41.23	1205.45	29.24	
98	2.14	41.28	1198.90	29.04	
97	2.14	41.28	1208.09	29.27	
96	2.14	41.25	1202.49	29.15	
95	2.14	41.28	1204.62	29.18	
94	2.14	41.26	1193.22	28.92	
93	2.14	41.26	1207.43	29.26	
92	2.14	41.29	1197.76	29.00	
91	2.14	41.29	1206.60	29.22	
90	2.14	41.28	1217.09	29.49	
89	2.14	41.28	1207.92	29.26	
88	2.14	41.26	1201.84	29.13	
87	2.14	41.24	1202.33	29.15	
86	2.14	41.24	1190.80	28.87	
85	2.14	41.23	1198.08	29.06	
84 (SmC)	2.14	41.15	1204.46	29.27	4.89
83	2.15	41.10	1183.15	28.79	
82	2.15	41.02	1186.49	28.92	
81	2.15	40.98	1201.68	29.33	
80	2.16	40.91	1201.51	29.37	
79	2.16	40.90	1206.94	29.51	
78	2.16	40.88	1201.35	29.39	
77	2.16	40.82	1190.49	29.17	
76	2.16	40.79	1194.84	29.29	
75	2.17	40.73	1196.63	29.38	
74	2.17	40.73	1199.07	29.44	
73	2.17	40.74	1199.72	29.45	
72	2.17	40.70	1199.72	29.47	
71	2.17	40.67	1194.85	29.38	
70	2.17	40.69	1206.94	29.66	
69	2.17	40.69	1211.58	29.77	
68	2.17	40.67	1208.43	29.72	
67	2.17	40.65	1217.43	29.95	
66	2.17	40.63	1220.29	30.03	
65	2.17	40.63	1223.84	30.12	
64	2.17	40.63	1227.08	30.20	
63	2.17	40.62	1233.77	30.38	
62	2.17	40.63	1242.98	30.59	
61	2.17	40.67	1238.27	30.45	
60	2.17	40.65	1237.40	30.44	

59	2.17	40.65	1237.57	30.44
58	2.17	40.65	1242.98	30.58
57	2.17	40.69	1240.18	30.48

N to SmA phase transition in **1/14**: The correlation length (ξ) and layer spacing (d-value) increased and as a result ξ/d value increased.
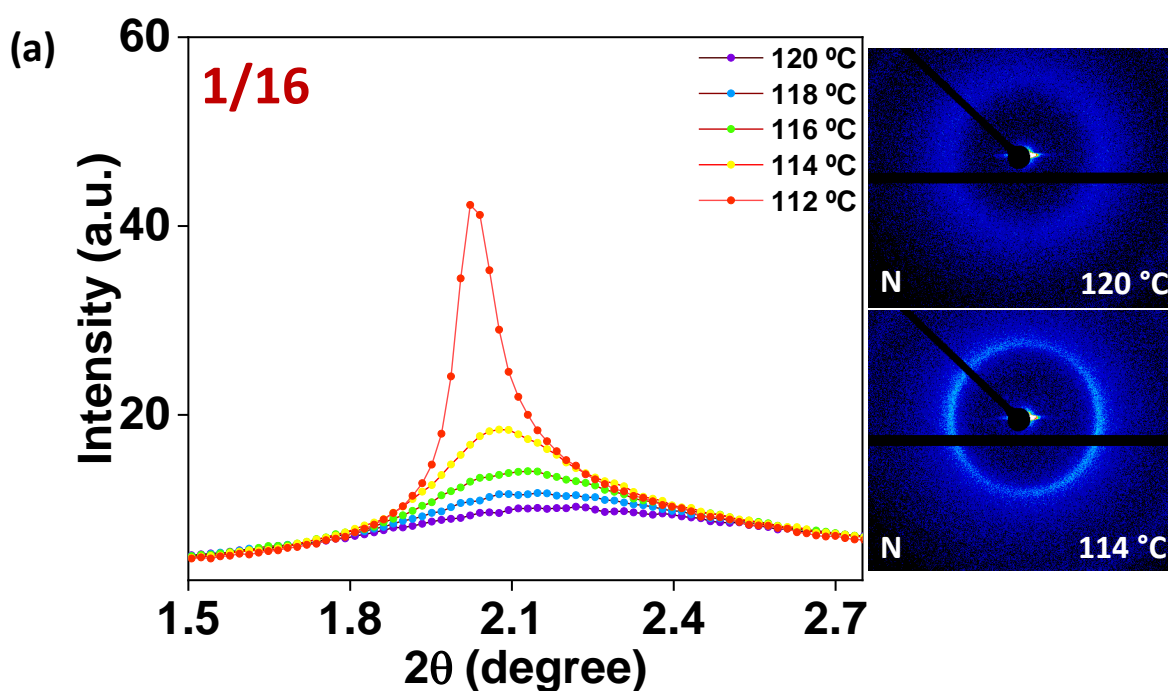
SmA to SmC phase transition in **1/14**: The layer spacing (d-value) decreased but correlation length (ξ) increased which resulted in an increased ξ/d value.

Layer shrinkage:

d_A (85 ˚C) = 41.23 Å, d_C (84 ˚C) = 41.15 Å

Layer shrinkage = [(d_A-d_C) / d_A] * 100 = **0.19 %**
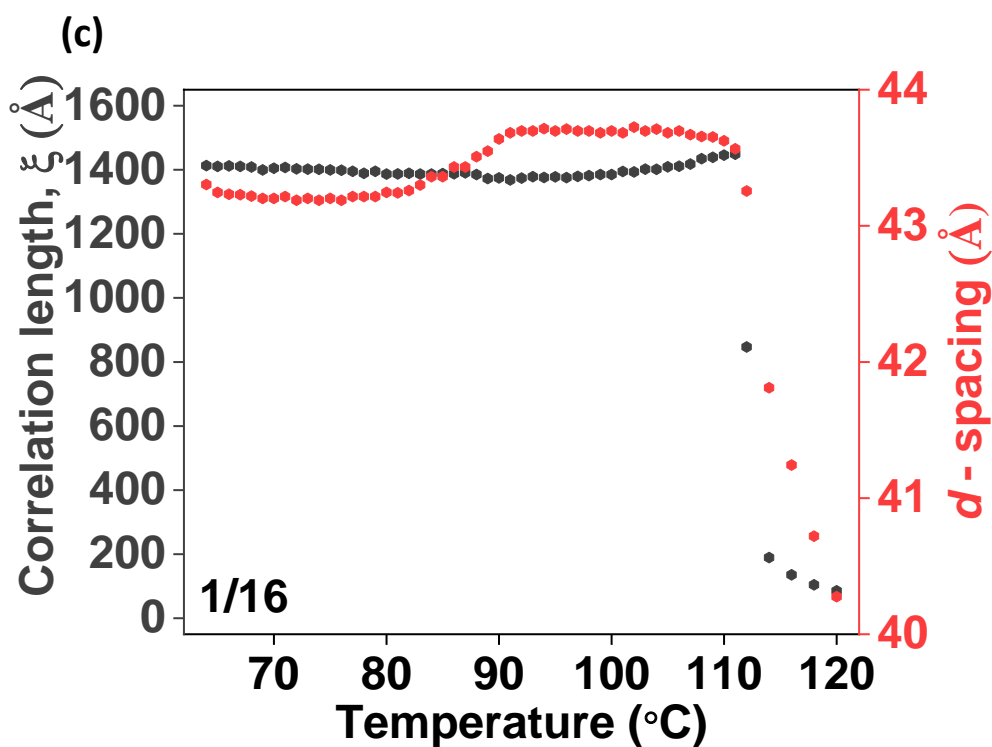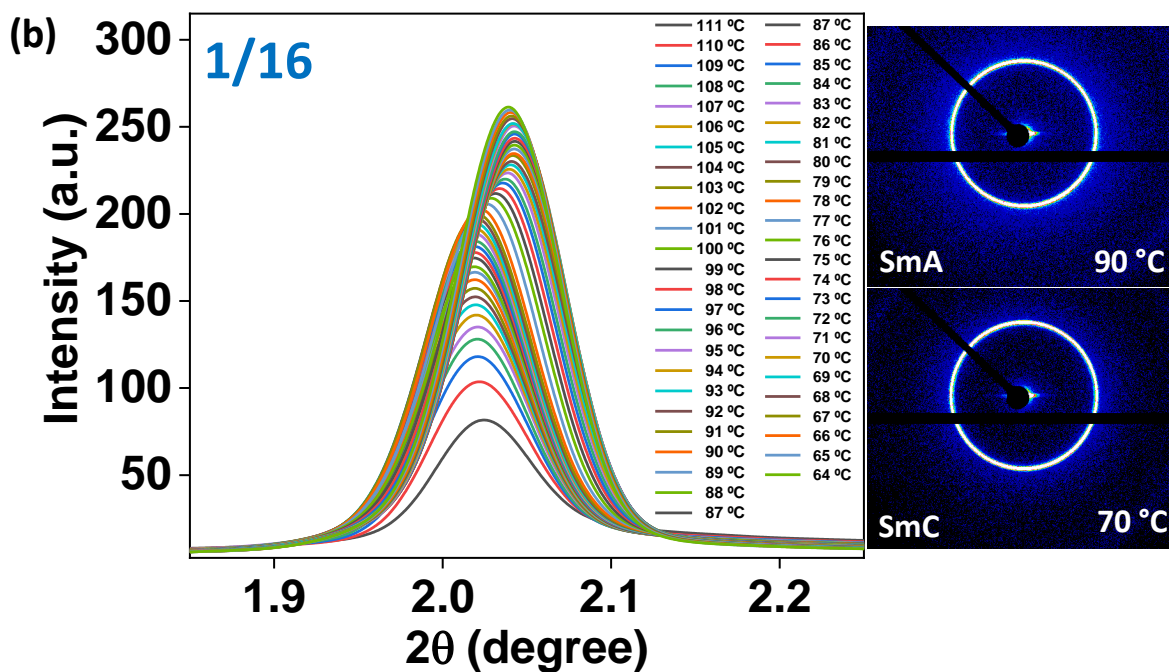
(d) Compound **1/16**:

Fig. S30 Intensity (a.u.) *vs.* 2θ (degree) profiles in the small-angle region (SAXS studies) for compound **1/16** in the cooling cycle displaying the (a) Nematic, (b) SmA, SmC phase (the 2D diffraction images are placed on the right). (c) Variation of correlation length (ξ) and *d*-spacing with temperature corresponding to the small angle peak of compound **1/16**.

Table S4. Record of 2θ (°), *d*-spacing (Å), correlation length *ξ* (Å) and number of correlated units (*ξ/d*) of the mesogens upon decreasing temperature corresponding to the first peak in the small-angle region in the XRD pattern of the compound **1/16**.

Temp (°C)	2θ (°) (small-angle)	*d*-spacing (Å) (small-angle)	*ξ* (Å)	*ξ/d*	*d*-spacing (Å) (wide-angle)
120 (N)	2.19	40.28	85.48	2.12	5.08
118	2.17	40.72	104.25	2.56	
116	2.14	41.24	135.47	3.28	
114	2.11	41.81	189.39	4.53	
112	2.04	43.26	846.76	19.58	
111 (SmA)	2.03	43.57	1448.60	33.25	5.04
110	2.02	43.62	1445.76	33.14	
109	2.02	43.65	1439.16	32.97	
108	2.02	43.66	1434.48	32.86	
107	2.02	43.67	1417.89	32.47	
106	2.02	43.70	1411.30	32.30	
105	2.02	43.68	1409.28	32.26	
104	2.02	43.71	1401.67	32.07	
103	2.02	43.70	1401.89	32.08	
102	2.02	43.72	1393.26	31.86	
101	2.02	43.68	1394.80	31.93	
100	2.02	43.70	1385.17	31.70	
99	2.02	43.68	1385.17	31.70	
98	2.02	43.70	1381.70	31.62	
97	2.02	43.70	1379.54	31.57	
96	2.02	43.71	1375.67	31.47	
95	2.02	43.70	1377.82	31.53	
94	2.02	43.71	1375.88	31.47	
93	2.02	43.70	1378.46	31.55	
92	2.02	43.70	1373.96	31.44	
91	2.02	43.68	1368.42	31.32	
90	2.02	43.64	1374.60	31.50	
89 (SmC)	2.03	43.55	1372.65	31.52	4.97
88	2.03	43.50	1385.17	31.84	
87	2.03	43.43	1390.63	32.02	
86	2.03	43.43	1387.79	31.95	
85	2.04	43.36	1388.22	32.02	
84	2.04	43.36	1386.48	31.98	
83	2.04	43.30	1386.70	32.02	
82	2.04	43.26	1388.88	32.10	
81	2.04	43.24	1386.92	32.07	
80	2.04	43.25	1386.48	32.06	
79	2.04	43.22	1395.47	32.29	

78	2.04	43.22	1388.88	32.14
77	2.04	43.22	1395.03	32.28
76	2.04	43.19	1398.57	32.38
75	2.04	43.20	1399.68	32.40
74	2.04	43.19	1401.45	32.45
73	2.04	43.20	1401.90	32.45
72	2.04	43.19	1402.79	32.48
71	2.04	43.22	1407.26	32.56
70	2.04	43.20	1404.80	32.52
69	2.04	43.20	1399.45	32.39
68	2.04	43.22	1408.84	32.60
67	2.04	43.23	1410.41	32.63
66	2.04	43.23	1411.99	32.66
65	2.04	43.25	1410.64	32.62
64	2.04	43.30	1413.12	32.63

N to SmA phase transition in **1/16**: The correlation length (ξ) and layer spacing (d-value) increased and as a result ξ/d value increased.
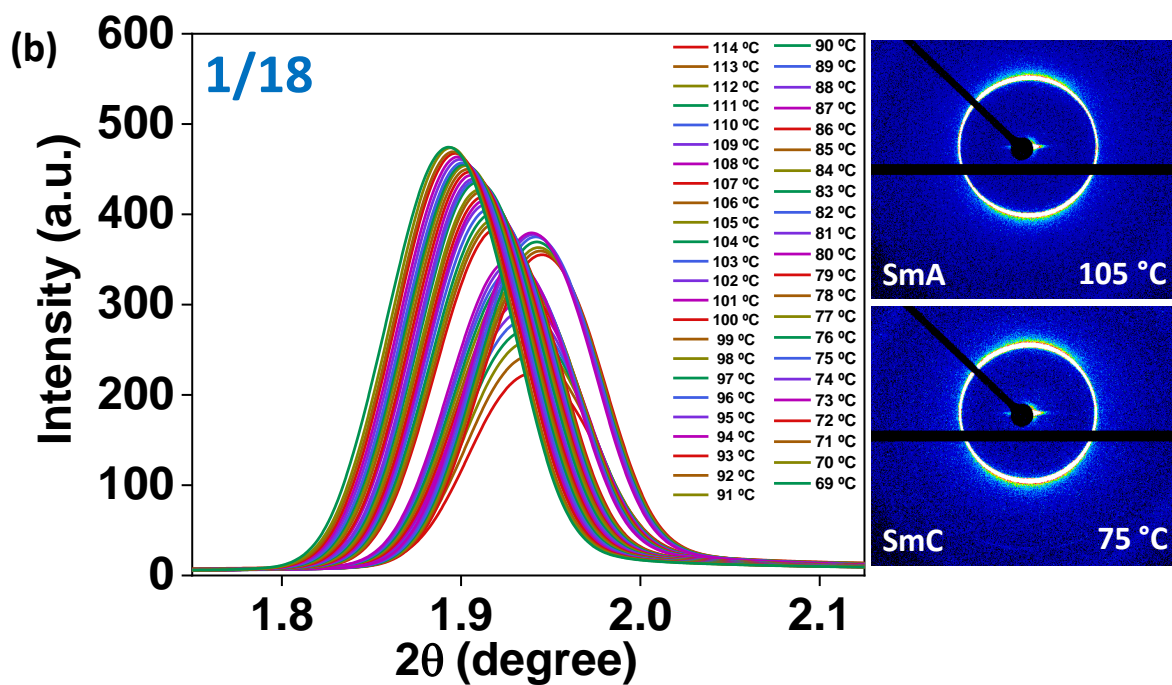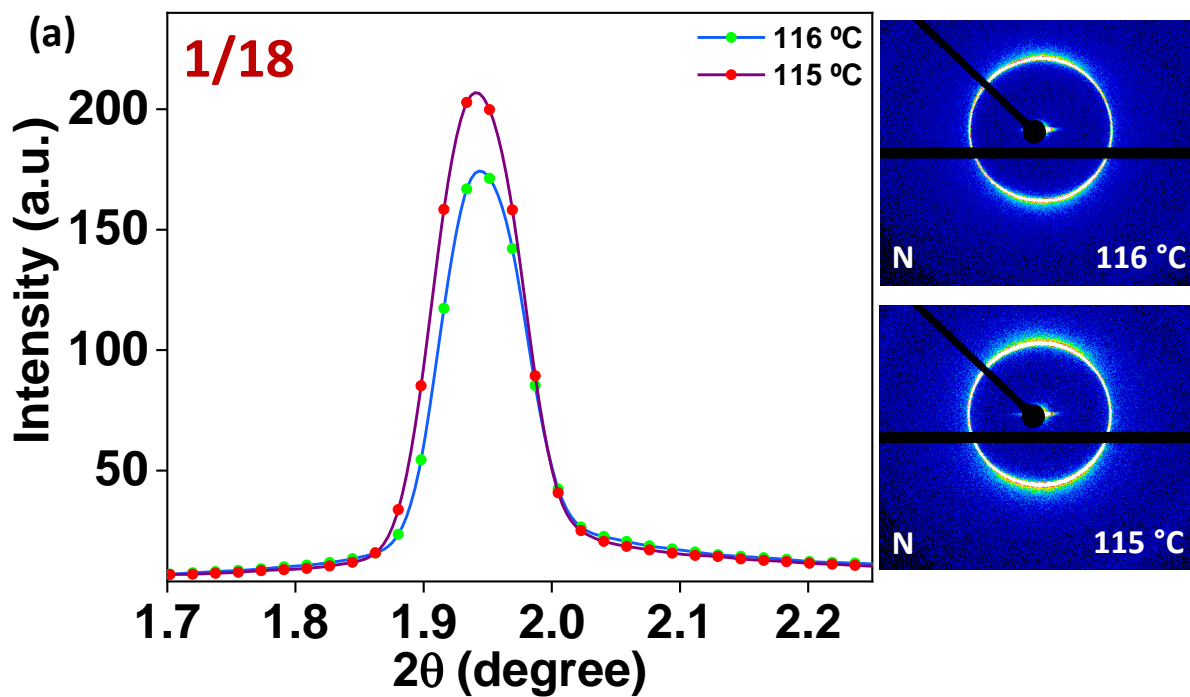
SmA to SmC phase transition in **1/16**: The layer spacing (d-value) decreased but correlation length (ξ) increased which resulted in an increased ξ/d value.

Layer shrinkage:

d_A (90 ˚C) = 43.64 Å, d_C (89 ˚C) = 43.55 Å

Layer shrinkage = [(d_A-d_C) / d_A] * 100 = **0.20 %**
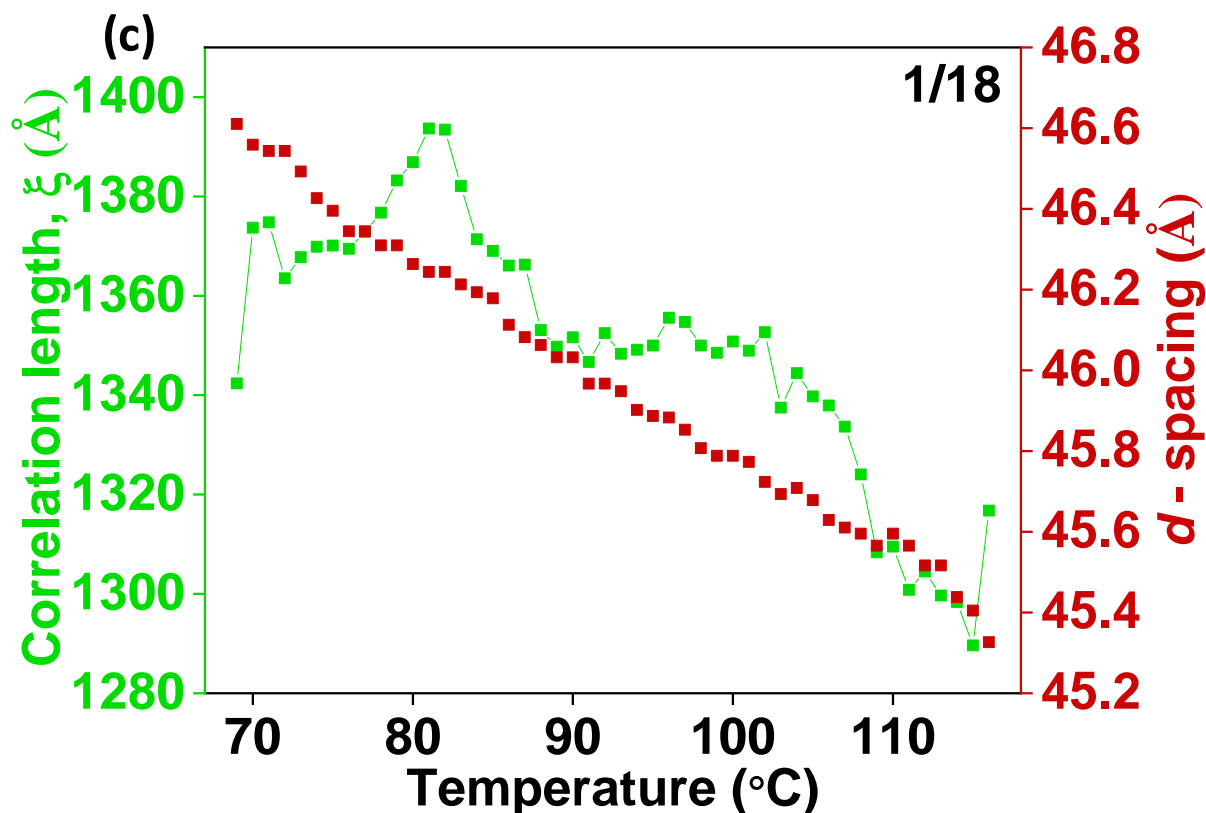
(e) Compound **1/18**:

Fig. S31 Intensity (a.u.) *vs.* 2θ (degree) profiles in the small-angle region (SAXS studies) for compound **1/18** in the cooling cycle displaying the (a) Nematic, (b) SmA, SmC phase (the 2D diffraction images are placed on the right). (c) Variation of correlation length (ξ) and *d*-spacing with temperature corresponding to the small angle peak of compound **1/18**.

Table S5. Record of 2θ (°), *d*-spacing (Å), correlation length ξ (Å) and number of correlated units (ξ/d) of the mesogens upon decreasing temperature corresponding to the first peak in the small-angle region in the XRD pattern of the compound **1/18**.

Temp (°C)	2θ (°) (small-angle)	*d*-spacing (Å) (small-angle)	ξ (Å)	ξ/d	*d*-spacing (Å) (wide-angle)
116 (N)	1.95	45.32	1316.74	29.05	5.09
115	1.94	45.40	1289.61	28.40	
114 (SmA)	1.94	45.43	1298.34	28.57	5.08
113	1.94	45.52	1299.68	28.55	
112	1.94	45.52	1304.48	28.66	
111	1.94	45.57	1300.83	28.55	
110	1.94	45.60	1309.51	28.72	
109	1.94	45.57	1308.35	28.71	
108	1.94	45.60	1324.05	29.04	
107	1.93	45.61	1333.66	29.24	
106	1.93	45.63	1337.90	29.32	
105	1.93	45.68	1339.73	29.33	

104	1.93	45.70	1344.42	29.41	
103	1.93	45.69	1337.50	29.27	
102	1.93	45.72	1352.67	29.58	
101	1.93	45.77	1348.95	29.47	
100	1.93	45.79	1350.80	29.50	
99	1.93	45.79	1348.53	29.45	
98	1.93	45.80	1349.98	29.47	
97	1.92	45.85	1354.74	29.55	
96	1.92	45.88	1355.58	29.54	
95	1.92	45.89	1349.98	29.42	
94 (SmC)	1.92	45.90	1349.15	29.39	4.98
93	1.92	45.95	1348.32	29.34	
92	1.92	45.97	1352.46	29.42	
91	1.92	45.97	1346.68	29.30	
90	1.92	46.03	1351.63	29.36	
89	1.92	46.03	1349.77	29.32	
88	1.92	46.06	1353.08	29.37	
87	1.91	46.08	1366.28	29.65	
86	1.91	46.11	1366.07	29.62	
85	1.91	46.18	1369.03	29.65	
84	1.91	46.19	1371.37	29.69	
83	1.90	46.21	1382.11	29.90	
82	1.90	46.24	1393.46	30.13	
81	1.90	46.24	1393.68	30.14	
80	1.90	46.26	1386.89	29.98	
79	1.90	46.30	1383.19	29.87	
78	1.90	46.30	1376.72	29.73	
77	1.90	46.34	1372.86	29.62	
76	1.90	46.34	1369.46	29.55	
75	1.90	46.40	1370.09	29.53	
74	1.90	46.42	1369.88	29.50	
73	1.90	46.49	1367.76	29.42	
72	1.90	46.54	1363.53	29.30	
71	1.90	46.54	1374.79	29.54	
70	1.90	46.56	1373.72	29.50	
69	1.89	46.61	1342.37	28.80	

SmA to SmC phase transition in **1/18**: The *d*-values constantly increased from 45.43-45.89 Å in the SmA phase (with *d*/L ~ 0.96) to 45.90-46.61 Å in the SmC phase (with *d*/L ~ 0.97); where, L = 47.9 Å is the molecular length of **1/18** in the most extended all-*trans* conformation of the terminal alkoxy chain. The observation of *d* < L in the SmA phase indicated the presence of "de Vries-like" phase. Upon cooling, the impact of increasing

packing density by alkoxy chain stretching on the layer spacing was more than the tilting of the mesogens, therefore, resulting in constant increment in the *d*-value.[3]

The correlation length (ξ) did not follow any trend upon decreasing temperature.

8.   Density Functional Theory (DFT) studies:

All the computations were performed with Gaussian 09 and GaussView 5.0 package.[4] Spin restricted DFT calculations with the B3LYP functional and the 6-311G (d, p) basis set[5,6] was carried out to optimize the geometry of all the compounds of **1/n** series. The bend angle was calculated to be 147° for all the compounds (Fig. S32) and deviated from the ideal 120° due to the transverse methyl group in the bent position of the central aromatic core. The components of the dipole moment and its resultant are presented in Table S6. The dipole moment (μ_x) and polarizability (α_{XX}) are significantly large in the X-direction.

The principal polarizability components (α_{XX}, α_{YY} and α_{ZZ}), isotropic polarizability component (α_{iso}), polarizability anisotropy ($\Delta\alpha$) and asymmetry parameter (η_α), relative to the molecular polarizability tensor α, calculated from DFT, are summarized in Table S7. The molecular polarizability component α_{XX} is comparatively larger along the molecular longitudinal X-axis for all the molecules than along the other two directions (Table S7). It may be noted that all the principal polarizability components and therefore, α_{iso} and $\Delta\alpha$ increase as the length of the terminal alkoxy chain (n = 10 to 18) increases. The asymmetry parameter η_α (~ 0.30) is small and the value is dependent on the bend angle i.e., 147°.

Table S6. DFT calculated dipole moment components (μ_x, μ_y, μ_z) and the resultant dipole moment (μ), bend angle and molecular length (L).

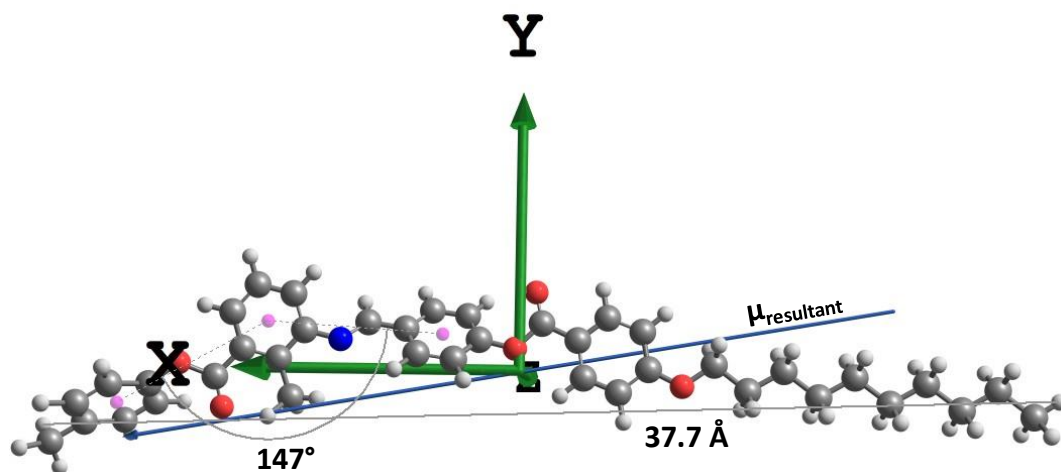| Compound	Dipole moment (Debye)				Bend angle (°)	Molecular Length, L (Å)
	μ_x	μ_y	μ_z	$\mu_{resultant} = (\mu_x{}^2 + \mu_y{}^2 + \mu_z{}^2)^{1/2}$		
1/10	4.98	0.85	0.38	5.07	147	37.7
1/12	4.99	0.91	0.37	5.09	147	40.2
1/14	4.99	0.96	0.37	5.10	147	42.8
1/16	4.99	1.00	0.37	5.10	147	45.3
1/18	4.99	1.05	0.37	5.15	147	47.9

Fig. S32 DFT optimized molecular structure of **1/10** in a Cartesian coordinate frame.

Table S7. DFT calculated principal polarizability components (α_{XX}, α_{YY}, α_{ZZ}), isotropic polarizability $\alpha_{iso} = (\alpha_{XX} + \alpha_{YY} + \alpha_{ZZ})/3$, anisotropy $\Delta\alpha = [\alpha_{XX} - (\alpha_{YY} + \alpha_{ZZ})/2]$ and asymmetry, $\eta_{\alpha} = [(\alpha_{YY} - \alpha_{ZZ})/(\alpha_{XX} - \alpha_{iso})]$. Parameters are relative to the molecular polarizability tensor in the Cartesian reference frame.

Compound	α_{XX}	α_{YY}	α_{ZZ}	α_{iso}	$\Delta\alpha$	η_{α}
1/10	883	405	296	528	532	0.30
1/12	914	424	319	552	542	0.29
1/14	949	445	337	577	558	0.29
1/16	983	465	356	601	572	0.29
1/18	1018	486	375	626	588	0.28

All polarizability components and anisotropy parameters are calculated in Bohr^3 (1 Bohr = 0.52917 Å).

9. Dielectric studies:

Temperature-dependent dielectric properties of compound **1/12** were studied in detail. Fig. S33 shows the variation of the parallel ($\varepsilon_{\parallel}$) and the perpendicular ($\varepsilon_{\perp}$) components of the dielectric constant. The dielectric anisotropy $\Delta\varepsilon = \varepsilon_{\parallel} - \varepsilon_{\perp}$ was found to be positive at all temperatures and its magnitude decreased as the temperature was lowered from N to SmC phase. Similar temperature dependence of the dielectric constants has been reported in several other asymmetric bent-core compounds (non-de Vries) exhibiting similar phase transition and attributed to the antiparallel correlation of longitudinal dipole component.[7] It may be noted that both $\varepsilon_{\parallel}$ and $\varepsilon_{\perp}$ varied smoothly across T_{AC}, without marking the phase transition. This is expected as the molecules in both the SmA and SmC phases are tilted.
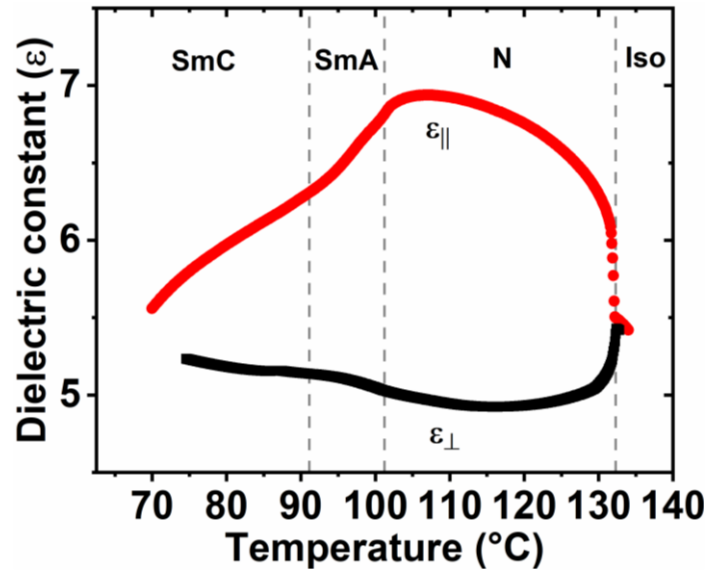
Fig. S33 Variation of parallel ($\varepsilon_{\parallel}$) and perpendicular ($\varepsilon_{\perp}$) components of dielectric permittivity with temperature. Phase transition temperatures are marked by vertical dotted lines. $\varepsilon_{\parallel}$ was measured in a homeotropic cell whereas $\varepsilon_{\perp}$ in a homogeneous cell with the applied voltage less than the Freedericksz's threshold voltage. Frequency f = 411 Hz, cell thickness 6 μm.

The dielectric dispersion at various temperatures was also studied in the frequency range of 100 Hz to 2 MHz. The perpendicular component ($\varepsilon_{\perp}$) did not show any dielectric relaxation whereas the parallel component ($\varepsilon_{\parallel}$) exhibited a single relaxation. Variation of the real and the imaginary parts of $\varepsilon_{\parallel}$ with angular frequency (ω) at three different temperatures corresponding to N, SmA and SmC phases are shown in Fig. S34a. The rapid increase in dielectric constant in the low frequency region was attributed to the ionic (impurity) contribution. In the intermediate frequency range, $\omega = 10^5$ to 2 x 10^6 rad/sec, it showed a dipolar type relaxation and the relaxation frequency decreased as the temperature reduced from the N to SmC phase. The data was fitted to the complex dielectric function, $\varepsilon_{\parallel}^*(\omega) = \varepsilon_{\parallel}'(\omega) + i\varepsilon_{\parallel}''(\omega) = \varepsilon_{\infty} + \frac{\Delta\varepsilon_1}{1+(i\omega\tau)^{1-\alpha}} + \frac{A}{\omega^n}$, where τ is the relaxation time, $\Delta\varepsilon_1 = \varepsilon_{\infty} - \varepsilon_s$ is the dielectric strength and A, n and α are constants. $\varepsilon_{\parallel}'(\omega)$ and $\varepsilon_{\parallel}''(\omega)$ are the real and imaginary parts of the dielectric constant. Fig. S34a also shows some representative fits to the experimental data. In all the fittings, α was found to be very small (< 0.01). The relaxation time, τ was obtained from the fitting at different temperatures. It strongly depends on temperature and can be fitted to the Arrhenius equation, $\tau = \tau_0 e^{\frac{U}{RT}}$ to obtain activation energy U, representing the energy barrier associated with the flip-over of the molecular long axis. Fig. S34b shows a linear plot of ln(τ) with the inverse of temperature (1/T). The activation energies of N, SmA were nearly equal and slightly larger than that of the SmC phase temperatures.
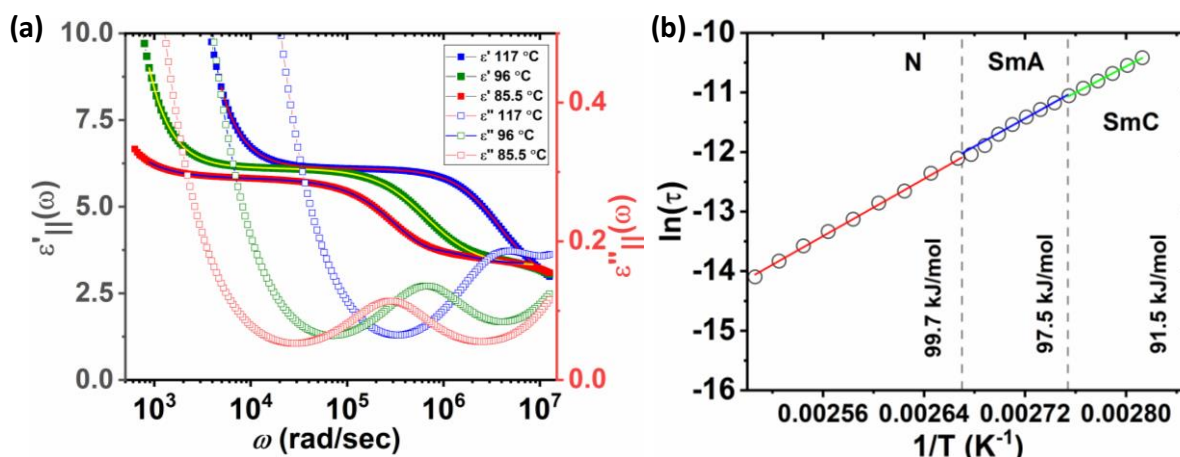
Fig. S34 (a) Variation of real $\varepsilon'_{||}(\omega)$ and imaginary $\varepsilon''_{||}(\omega)$ parts of the dielectric permittivity measured in a homeotropic cell with angular frequency ω. Solid lines are theoretical fits to the real component. (b) Linear plot of $\ln(\tau)$ with 1/T.

In compound **1/12**, temperature-dependent splay (K_{11}) and bend (K_{33}) elastic constants in the nematic phase were also measured. An electro-optic technique was adapted wherein the optical retardation of a planar sample was measured as a function of applied ac voltage.[8] The splay elastic constant K_{11} was obtained directly from the Freedericksz's threshold voltage and K_{33} was obtained from fitting the data with a theoretical model.[9] Fig. S35 shows temperature dependence of K_{11} and K_{33}. Except very close to N-Iso and N-SmA transitions, $K_{33} < K_{11}$ at all other temperatures (inset of Fig. S35). Below the N-Iso transition, both increased with decreasing temperature, in addition, K_{33} showed a strong pre-transitional divergence as the N to SmA transition approached. Similar temperature dependence was also observed in many bent-core compounds.[10] Lower value of K_{33} was attributed to the coupling of the molecular shape (bent) with the bend distortion. The pre-smectic divergence of K_{33} occurred due to the strong suppression of bend fluctuations as the N-SmA transition temperature approached.[10]
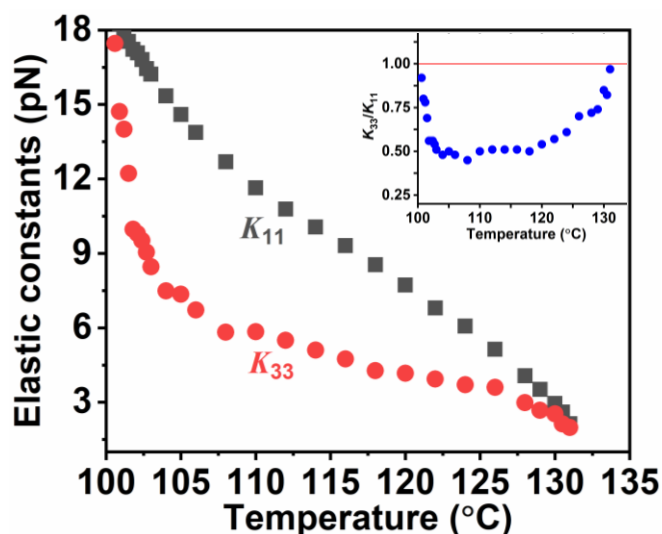

Fig. S35 Variation of splay (K_{11}) and bend (K_{33}) elastic constants with temperature in the nematic phase. Inset shows variation of the ratio K_{33}/K_{11} with temperature.

Further, the effect of electric field in the SmA phase was studied (Fig. S36). When the field was applied perpendicular to the director, the color change in the texture was observed with increasing field, and it became completely dark, i.e., homeotropic at 46 V. This suggested that this phase was not SmC alpha type because the molecules are tilted in SmC alpha and the phase is weakly biaxial. Hence, it was not expected to get complete dark state (homeotropic) under electric field in SmC alpha phase. When low frequency ac voltage was applied to compound **1/12**, some dielectric response was observed but no ferroelectric-like switching response. Therefore, the possibility of short-pitch smectic C alpha phase could be ruled out.
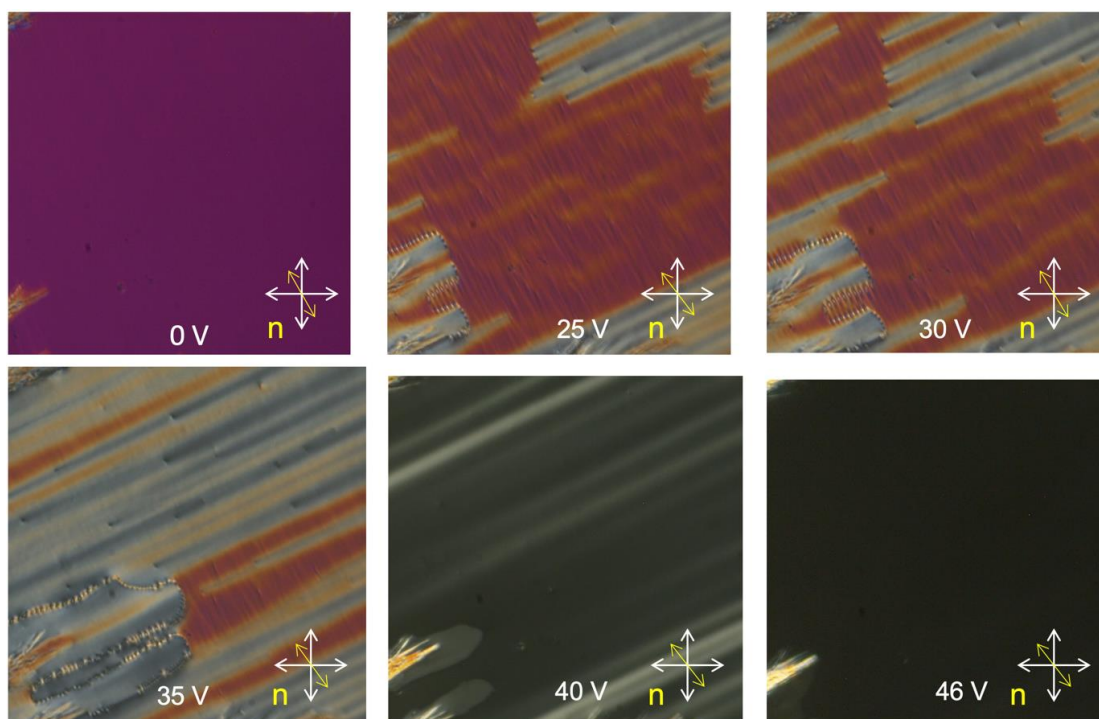

Fig. S36 Effect of ac electric field in the SmA phase of compound **1/12** at T = 95 °C. Double headed yellow arrow indicates the rubbing direction. Frequency of the field = 3.11 kHz. Cell thickness 3.5 µm.

10. Materials and reagents:

All chemicals and solvents were all of AR quality and were used without further purification. 4-Hydroxybenzaldehyde, 3-amino-2-methylbenzoic acid were all purchased from TCI (Japan); N, N-dicyclohexylcarbodiimide (DCC) from Fluka Analytical; 4-dimethylaminopyridine (DMAP), n-bromoalkanes, glacial acetic acid and potassium hydroxide from Sigma Aldrich; 4-hydroxybenzoic acid from Himedia; absolute ethanol and p-cresol from Merck. Column chromatographic separations were performed on silica gel (100-200 mesh). Thin layer chromatography (TLC) was performed on aluminium sheets pre-coated with silica gel (Merck, Kiesegel 60, F254).

11.   Instrumental:

The instrumental details for structural characterization are similar to as mentioned in our previous reports[1,2] and briefed here for the reader's convenience.

"Structural characterization of the compounds was carried out with a combination of FT-IR (Infrared Spectroscopy-Perkin Elmer Spectrum AX3), UV-Vis-NIR spectrophotometer (LABINDIA UV-Vis Spectrophotometer 3000+), High Resolution Mass Spectrometry (Waters synapt g2s), ^{1}H-NMR and ^{13}C-NMR (Bruker Biospin Switzerland Avance-iii 400 MHz and 100 MHz spectrometers, respectively). NMR spectra were recorded using deuterated chloroform ($CDCl_3$) as solvent and tetramethylsilane (TMS) as an internal standard. Polarizing Optical Microscopy (POM) textural observations of the mesophases were performed with Nikon Eclipse LV100POL polarizing microscope provided with a Linkam heating stage (LTS 420) and the images were captured using a Q-imaging camera. Differential Scanning Calorimetry (DSC) measurements were performed on Perkin Elmer DSC 8000 coupled to a Controlled Nitrogen Accessory (CLN2) with a scan rate of 10 $^\circ$C min^{-1} both on heating and cooling. X-ray Diffraction (XRD) studies were carried out on samples using CuKα (λ=1.54 Å) radiation from GeniX3D microsource operating at 50 kV and 0.6 mA, using Pilatus 200K detector in Xeuss 2.0 SAXS/WAXS system."

12.   References:

1.   S. Kaur, G. Mohiuddin, P. Satapathy, R. Nandi, V. Punjani, S. K. Prasad and S. K. Pal, *Mol. Syst. Des. Eng.*, 2018, **3**, 839-852.
2.   S. Kaur, G. Mohiuddin, V. Punjani, R. K. Khan, S. Ghosh and S. K. Pal, *J. Mol. Liq.*, 2019, **295**, 111687 (1-11).
3.   S. P. Sreenilayam, Y. P. Panarin, J. K. Vij, V. P. Panov, A. Lehmann, M. Poppe, M. Prehm and C. Tschierske, *Nat. Commun.*, 2016, **7**, 11369 (1-8).
4.   M. J. Frisch, et al., Gaussian 09, Revision B.01, Gaussian, Inc., Wallingford CT, 2010.
5.   K. Kim and K. D. Jordan, *J. Phys. Chem.*, 1994, **98**, 10089-10094.
6.   P. J. Stephens, F. J. Devlin, C. F. Chabalowski and M. J. Frisch, *J. Phys. Chem.*, 1994, **98**, 11623-116.
7.   P. Sathyanarayana, S. Radhika, B. K. Sadashiva and S. Dhara, *Soft Matter*, 2012, **8**, 2322-2327.
8.   S. W. Morris, P. Palffy and D. A. Balzarini, *Mol. Cryst. Liq. Cryst.*, 1986, **139**, 263-280.
9.   P. Sathyanarayana, M. C. Varia, A. K. Prajapati, B. Kundu, V. S. S. Sastry and S. Dhara, *Phys. Rev. E*, 2010, **82**, 050701(R).
10.   P. Sathyanaraya, M. Mathews, Q. Li, V. S. S. Sastry, K. V. Le, H. Takezoe and S. Dhara, *Phys. Rev. E*, 2010, **81**, 010702(R).